Digital Discovery

Check for updates

Computational and data-driven modelling of solid polymer electrolytes

Kaiyang Wang, [a] Haoyuan Shi, [b] Tianjiao Li, [b] Liming Zhao, [b] Hanfeng Zhai,[b] Deepa Korani[a] and Jingjie Yeo [*ab]

Solid polymer electrolytes (SPEs) have been regarded as a safer alternative for liquid electrolytes in rechargeable batteries, yet they suffer from drawbacks such as low ionic conductivity. Designing SPEs with optimal performance is a challenging task, since the properties of SPEs are influenced by parameters across multiple scales, which leads to a vast design space. The integration of theory-based modeling methods and data-driven approaches can effectively link chemical and structure features of SPEs to macroscopic properties. Machine learning (ML) algorithms are paramount to data-driven modeling. This review aimed to highlight the ML algorithms used for SPE design, and how these algorithms can be employed synergistically with theory-based modelling methods such as density functional theory (DFT), molecular dynamics (MD) and coarse graining (CG). In addition, this work is concluded with our outlook in this young and promising field.

1 Introduction

The past few decades have witnessed the great success of rechargeable batteries. The commercialization of lithium-ion batteries since the 1990s have shaped our life in multiple aspects: from portable electronics to electric vehicles, from medical devices to power grids.[1] With the continuous upsurge in demand for energy storage, future batteries will require ever-improving energy density and product safety.[2] As an indispensable component in the battery, electrolytes play a key role in conducting ions and insulating electrons. At present, many battery systems on the market adopt liquid electrolytes since they offer benefits of high ionic conductivity and excellent wetting of electrode surfaces. Nevertheless, liquid electrolytes suffer from inadequate electrochemical and thermal stabilities, low ion selectivity, and poor safety.[3] To circumvent the drawback of liquid electrolytes, researchers have delved into

[a]*Department of Materials Science and Engineering, Cornell University, Ithaca, NY 14853, USA*

[b]*Sibley School of Mechanical and Aerospace Engineering, Cornell University, Ithaca, NY 14853, USA. E-mail: jingjieyeo@cornell.edu*

Kaiyang Wang is currently a PhD candidate in Materials Science and Engineering (MSE) with a minor in Computer Science at Cornell University. He graduated with a bachelor's degree in MSE from Tsinghua University in 2017. Subsequently, he received his master's degree from Cornell University in 2019 and his thesis focused on 3D printing and soft matter. He developed a keen interest in computational materials science

Kaiyang Wang

since diving into the PhD program. He is particularly passionate about the intersection of machine learning and materials design.

Prof. Jingjie Yeo is an assistant professor in Cornell University's Sibley School of Mechanical and Aerospace Engineering. His lab uses multiscale computational mechanics and materials science to engineer dynamically-responsive, living materials through interdisciplinary studies of materials and biological phenomena for applications in engineering and biomedicine. Since 2018, he has been a co-instructor in Station1, a social

Jingjie Yeo

nonprofit organization dedicated to building the foundations of the university of the future through educational opportunity and socially-directed frontier STEM education, research, and internships.

developing solid electrolytes that are generally considered safer. There are three state-of-art solid electrolytes: inorganic, polymer, and composite. Among them, solid polymer electrolytes (SPEs) consist of a polymer matrix as a host and alkali metal salts in a solvent-free environment. Compared to the inorganic solid electrolytes, SPEs can endow the batteries with high safety, good processibility, and enhanced mechanical compliance with the electrodes.[4] However, one of the major obstacles for SPEs is their low ionic conductivity, which is closely related to the segmental motion of polymer chains. Most SPEs have ionic conductivities of less than 10^{-5} S cm^{-1} under room temperature and Li$^+$ transference numbers of around 0.2–0.5.[5] In comparison, SPEs for lithium batteries should be above 10^{-5} S cm^{-1} to ensure practical operation.[6] Since it is non-trivial to directly infer ionic conductivity given a polymer structure, researchers have proposed some subordinate parameters to consider. Two crucial parameters are the glass transition temperature (T_g) and the ion-pair dissociation ability.[7] Lower T_g guarantees high chain mobility under room temperature, and easier ion-pair dissociation enables fast Li$^+$ transport. In addition to low ionic conductivity, there are several other properties that require enhancement. SPEs should also have good electrochemical stability to minimize high voltage oxidation at the cathode interface.[8] The polymer redox window of SPEs are expected to withstand at least 4 V *versus* Li/Li$^+$ and preferably 4.5 V, which enables Li$^+$ extraction from an oxide host cathode without oxidation of the electrolyte in a 4 V cell during a charge/discharge cycle.[9,10] The mechanical properties should also be another key property to consider. SPEs with high modulus have shown large resistance for dendrite growth at Li anode in Li-metal batteries, which can be explained by Newman and Monroe model.[11–13]

To date, researchers have investigated various kinds of SPE materials, such as polyethylene oxide (PEO), polyacrylonitrile (PAN), polymethyl methacrylate (PMMA) and polyvinyl alcohol (PVA). However, it is difficult to propose an overall satisfying performance using a homopolymer. For example, PEO suffers from electrochemical instabilities at high voltages and low ionic conductivity at room temperature.[14] Researchers have made new attempts such as incorporating plasticizers or nanofillers, employing block copolymers, and engineering polymer structures.[15–19] As the material systems for SPE become more sophisticated, finding an optimal SPE is essentially a task that needs to be tackled from multiple aspects in a vast design space. As displayed in Fig. 1, it requires searching and optimization of physicochemical parameters across multiple scales, such as local interactions, chain dynamics and thermodynamics.[20,21] There is no single index that is sufficient to describe the performance of an SPE material for all the polymers.[22]

With the rapid growth of computational power, employing computational and data-driven modelling methods to facilitate the exploring and designing process has become an appealing choice to greatly accelerate the trial-and-error cycle and minimize experimental costs.[23] Over the past few decades, computational methods such as density functional theory (DFT) have been used synergically with experimental methods to aid battery development, particularly in material modelling and screening. However, these methods can be intensive on computational resources.[24] With the exciting progress of data science in the past decades, screening, prediction, optimization, and design tasks among a large number of candidates have become more tractable. Data-driven approaches are sometimes referred to as the fourth paradigm in materials discovery.[25] They can provide great flexibility by automatically discovering patterns in datasets using algorithms, without the need for extensive domain knowledge.[26] There are two major routes to establish databases: one is through the experimental paradigm, *i.e.*, collecting data from literature or performing
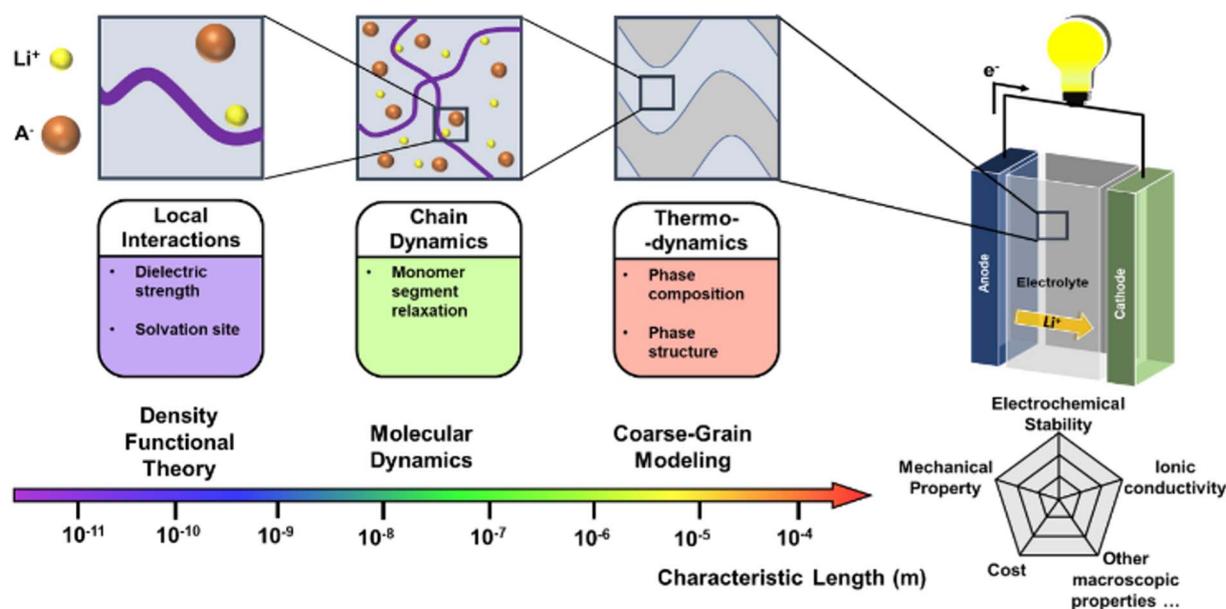

Fig. 1 The macroscopic properties of SPE are related to physicochemical parameters across different scales, which correspond to different computational techniques highlighted in this article.

experiments to measure desired properties; another is through the computational paradigm, *i.e.*, using computational methods to calculate material properties. Due to the complexity of the design space and high cost, the coupling of computational methods and data-driven approaches are becoming a popular trend for addressing challenges in modelling SPEs.

Herein, we are hoping to provide insights for both experimentalists and theorists in this area and foster more collaboration between them to facilitate the development of advanced SPEs. As such, our review primarily emphasizes the methodologies of computational and data-driven techniques, with examples on how they are employed in the SPE system. First, we review some basic concepts about machine learning (ML), including frequently used algorithms and how they are applied to material modelling, with an emphasis on screening and prediction. Subsequently, we review optimization algorithms that are commonly used for materials design. We are providing specific examples on how certain algorithms are tailored to SPE research. Next, we discuss how data-driven methods are incorporated into computational simulation tools, such as density functional theory (DFT), molecular dynamics (MD), and coarse graining (CG). Lastly, we provide a summary and outlooks on using computational and data-driven approach for modelling of SPEs.

2 ML fundamentals

2.1 Basic concepts of ML

Machine learning (ML) is a subfield of artificial intelligence that refers to algorithms and programs that demonstrates "intelligence" like humans, *i.e.*, improves with training.[27] Compared to theory-driven modelling methods, ML algorithms can extract useful relationships directly from a dataset without being given explicit instructions of how to analyze or draw conclusions from the data.[28] Thus, ML-based modeling is often used interchangeably with "surrogate modeling" in the realm of engineering.[29] Generally, there are three types of ML: supervised learning, unsupervised learning, and reinforcement learning.[30] The goal in supervised learning is to make predictions from labelled data. For supervised learning, there are two common tasks for a problem according to the types of output: classification and regression. The classification task establishes a mapping function from input variables to discrete output values, such as polymer chain configurations.[31,32] In comparison, the regression task maps input to continuous output values or physical quantities such as glass transition temperature, ionic conductivity, and potential energy surfaces (PES). A special case of supervised learning is called transfer learning, where a model is pretrained on one task and repurposed for another related task.[33,34] The merits of transfer learning lie in dealing with small training sets and saving training time. Compared to supervised learning, unsupervised learning addresses problems containing only input data with no corresponding labels. The goal in unsupervised learning is to uncover structure in the data themselves.[28] Unsupervised learning tends to be more subjective than supervised learning: the conclusion to an unsupervised learning problem is not

rigorously determined and is intimately tied to the algorithm we choose. Unsupervised learning can be applied in data visualization, dimensionality reduction, clustering, exploratory data analysis, and so on. For instance, clustering can be used to group data to identify common features, and exploratory data analysis can help to detect patterns and anomalies.[35,36] Reinforcement learning (RL) is concerned with building an intelligent agent that can interact with the environment and has been used in areas such as robotic control and music generation.[37,38] For a reinforcement learning problem, we define a reward (a scalar feedback signal) indicating how well the agent is doing at every step. The goal of reinforcement learning is to maximize the expected cumulative reward. At every step, the agent executes an action, receives an observation, and receives a scalar reward; in comparison, the environment receives an action, emits an observation, and emits a scalar reward. When the environment is fully observable to the agent, this whole process is a Markov decision process. To build an RL agent, one may include one or more of the components: policy, which describes an agent's behavior; value function, which describes how good each state or action is; and model, which describes the agent's representation of the environment. For chemistry applications, reinforcement learning techniques are being increasingly used to search for molecules with desired properties in large chemical spaces.[39,40]

Loss function, or sometimes called objective function or risk function, is a function that measures the performance of the ML model. The goal of ML is often to efficiently establish a model to minimize the loss function. Although there are some classic loss functions available such as squared loss, absolute loss, zero-one loss, exponential loss, Hinge loss and Huber loss,[41,42] researchers have developed many task-dependent loss functions. For instance, Mardt *et al.* designed variational approach for Markov processes (VAMP) loss to measure the consistency between different time steps in molecular dynamics (MD) simulations.[43] When evaluating an ML model, the total error can be decomposed into three principal terms: variance, bias, and noise as indicated in Fig. 2a.[27,40] Variance captures how "specialized" the model is to a particular training set. Bias describes the inherent error of the model even with infinite training data. Noise measures ambiguity due to data distribution and feature representation, and it comes as an intrinsic aspect of data. When optimizing the model, there often exists bias-variance tradeoff as indicated in Fig. 2b.[40] If the model has high bias and low variance, the model is "underfitting" and not able to sufficiently capture data features. If the model has low bias and high variance, the model is "overfitting" and introduced unnecessary complexity. To diagnose whether the model is suffering from the above issues, we usually split our data into three sets: training set, validation set and test set. The training set is used for "learning" the model, whereas the validation set is to help validate if the loss obtained from the training is reliable. The test set simulates how the model interacts with the future unseen data. A good ML model should have both low bias and low variance, which is usually indicated *via* a low error in both training and validation sets.
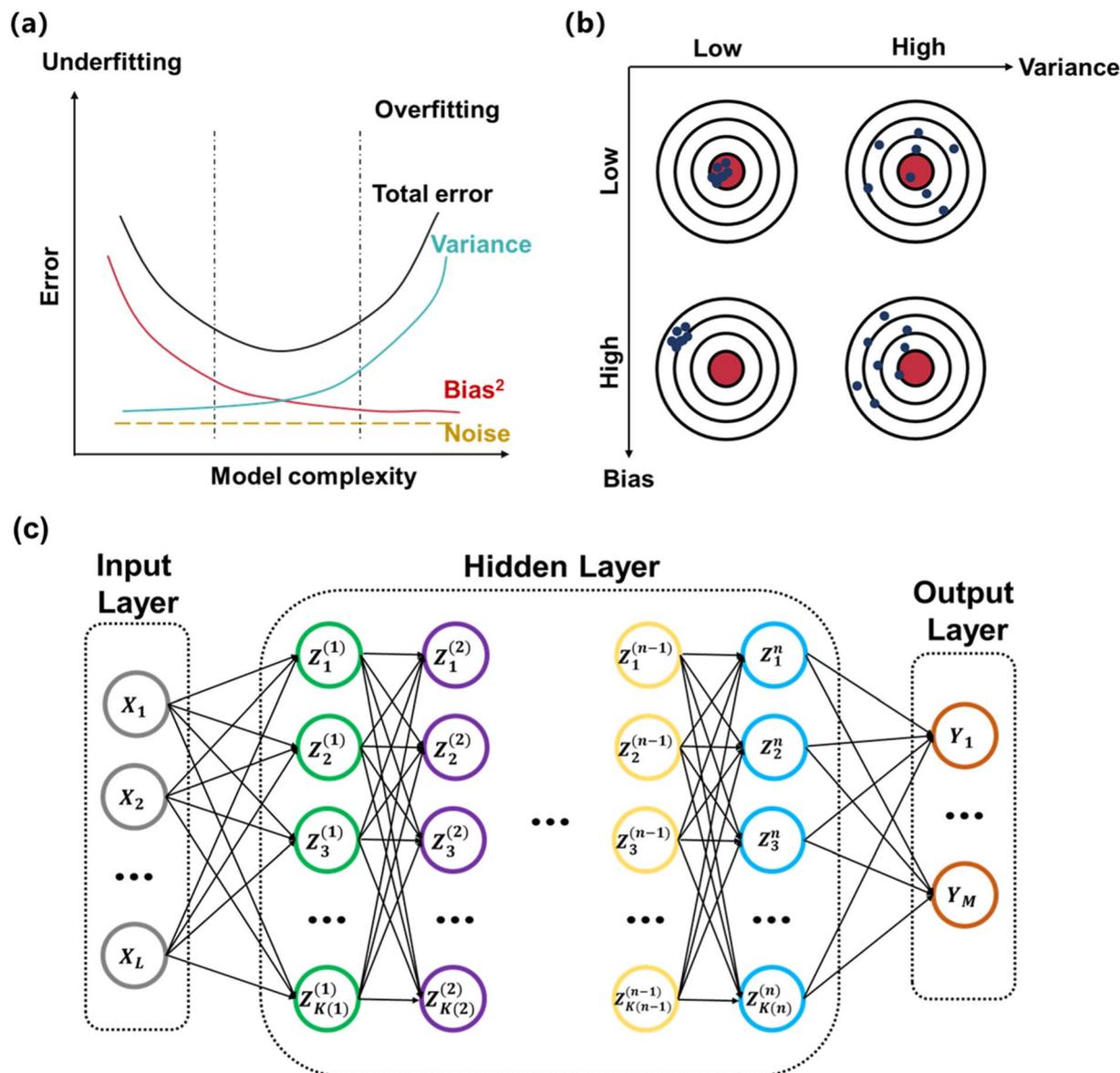
Review

Digital Discovery

Fig. 2 (a) The relationship between total error, variance, bias, and noise. (b) A graphic demonstration of bias–variance tradeoff. (c) The typical architecture of a feed-forward network.

Neural networks (NNs) are an important type of ML algorithm inspired by the biological neural networks that constitute animal brains.[44] Fig. 2c displayed the architecture of a feed forward neural network, where the information flows in only one direction. Each circle in the network is a datapoint called a neuron. There are three layers in this network: input layer, hidden layer, and output layer. For every layer, the data is updated in the following way:

$$z_i^{(k)} = g\left(\sum_j W_{i,j}^{(k-1,k)} z_j^{(k-1)}\right) \quad (1)$$

where $z_i^{(k)}$ is the ith updated value in layer k, z_j^{k-1} is the jth value from the layer $k-1$, and $W_{i,j}^{(k-1,k)}$ is the weight that connects

$z_i^{(k)}$ to $z_j^{(k-1)}$, and g is a nonlinear function (often referred to as activation function). Intuitively, each neuron gathers information from the neurons that connect to it *via* a linear combination, then performs a non-linear transformation. For a given neural network, the goal is to learn the weights among the neurons such that the loss function is minimized. Some of the common choices of activation functions can be sigmoid function, hyperbolic tangent, and rectified linear unit (ReLU). The power of NNs roots from the universal function theorem, which guarantees that NNs with enough neurons and number of layers can represent and approximate any complex function given sufficient data and training time.[45] In the next section, we are going to discuss some frequently used NN algorithms.

2.2 Basic concepts of ML

2.2.1 Graph neural networks (GNN). Graph Neural Networks (GNNs) are neural networks operated upon graphic data structures. A graph can be utilized to encode information and relationships among data points through its attributes: node attributes, edge attributes, and global attributes. For example, graphs can store information of molecules, where nodes can represent individual atoms and edges can represent bonds.[46] GNNs are optimizable transformations on all attributes of the graph with permutation invariances, *i.e.*, the connectivity of the graphs preserves during transformations.[47] In a GNN, the information can be embedded or processed on an edge level, node level or a global level, which offers great flexibility to data processing. To achieve message passing between different parts of the graph or make predictions based on a specific part of the graph, we normally apply a technique called pooling. Fig. 3a exhibited an example of pooling, for each node in the graph, one can gather information from all its neighboring nodes and aggregate the information using an aggregation function. Subsequently, the aggregated result is passed through a transform function to complete one update step of the current node. After the update, the node not only possesses the information about itself, but also incorporates the information from its first neighbors. We can infer that the
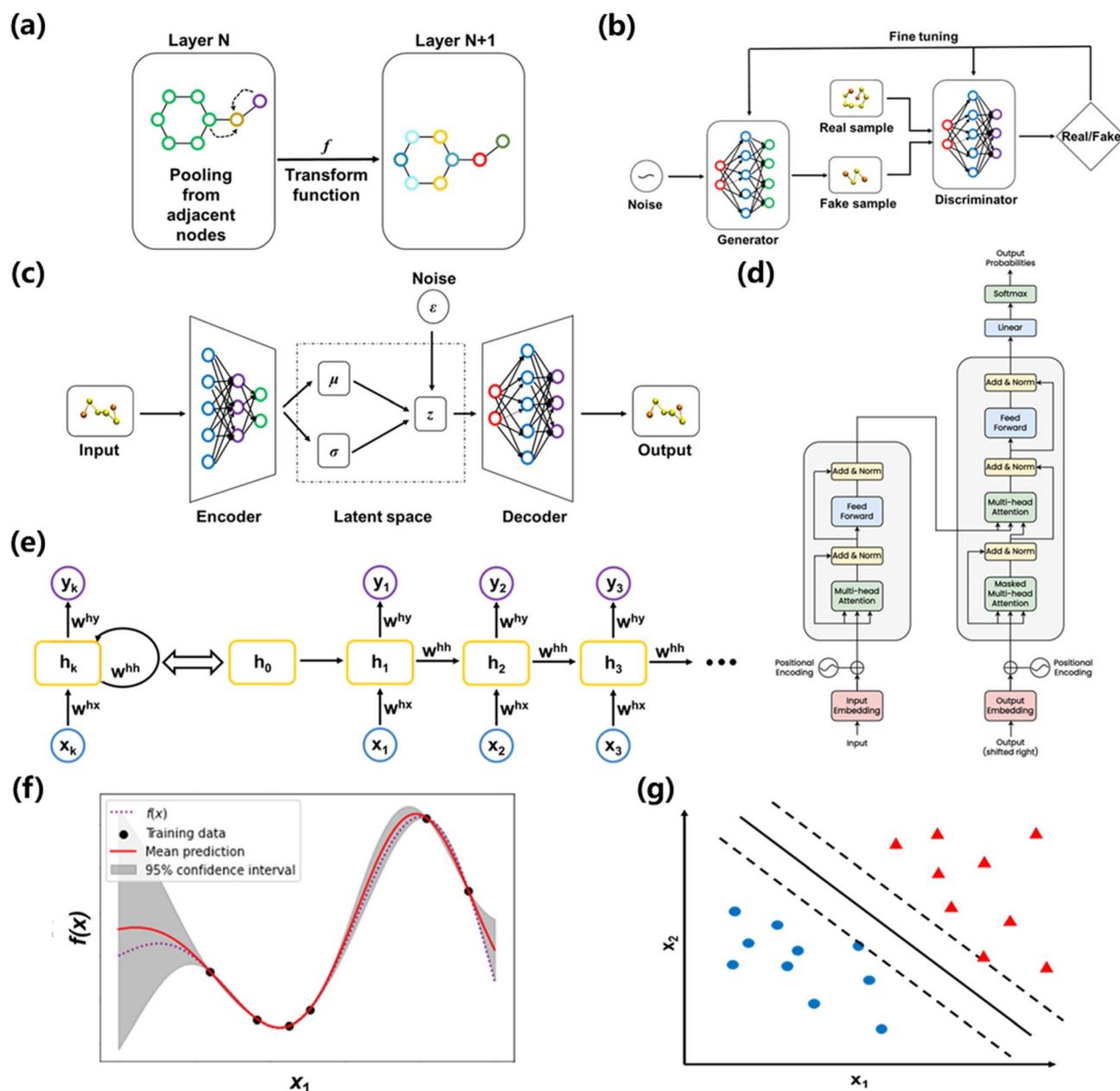

Fig. 3 (a) Message passing of a GNN network from layer N to layer $N + 1$. (b) GAN architecture. (c) VAE architecture. (d) RNN architecture. (e) Transformer architecture. (f) A graphic demonstration of GP regression. (g) A graphic demonstration of SVM.

information is passed between nodes of the graph if such operation is performed multiple times. Occasionally, to deal with a large graph or account for the effects of distant nodes, a "master node" that connects all the nodes in the graph can be added to a GNN.

Due to its versatile functions, GNNs have been successfully applied in both supervised and unsupervised learning scenarios in material science, such as feature engineering of molecules, discovery of hidden dynamics, visualization of material databases, prediction of material properties, and generation of force fields. Xie *et al.* developed a GNN to visualize the similarities of crystals.[48] They encoded the elements as well as the lattice structure to graph data. Since the information of the Kth-order neighbor can be described by K operations of the GNN, they exploited the output vectors to represent local environments of atoms. Plotting of the as-learned vectors can then provide insights on certain patterns from a material database. Coley *et al.* used GNNs to predict major products of organic reactions based on the reactant, reagent, and solvent species.[49] They embedded the atomic number, formal charge, bond order and other molecular information of a reaction to a graph as an input to a GNN. For a particular molecule, the GNN learned to calculate likelihood scores for each bond change between each atom pair, which was represented *via* the change of connectivity in a graph. After using 410k, 30k and 40k reactions as training, validation and testing data points, the model was compared to human benchmark and the prediction accuracy was quite close. Batzner *et al.* proposed a GNN for learning MD interatomic potentials called E(3)-equivariant GNN.[50] Since some properties of an atomic system such as radial distribution function and potential energies do not change under translation or rotation transformation, this permutation invariance naturally matches the property of an GNN. *Via* subtly designed atomic embeddings and convolution layers, their network architecture brings tremendous advantages in data efficiency, requiring up to 1000 times less training data than its precedents.

2.2.2 Generative adversarial networks (GAN). Generative Adversarial Networks (GAN) consist of two networks playing an adversarial game against each other. Different from a typical feed forward NN, GAN is a type of implicit generative algorithm instead of a discriminative algorithm, which generates new samples *via* estimating the underlying true distribution from data. Concretely, GANs do not provide a model function as the output, but rather produce "sample-like" data. Fig. 2b exhibits the architecture of a GAN; one network is called the "generator", and the other network is called "discriminator". During the training process, the loss functions of GAN can be expressed as:[51]

$$\min_G \max_D V(D, G) = \mathbb{E}_{x \sim p_{\text{data}}(x)}[\log D(x)] + \mathbb{E}_{z \sim p_z(z)}[\log(1 - D(G(z)))]$$

(2)

The min–max function reflects the adversarial relationship between the two networks: the goal of the discriminator is to maximize the prediction accuracy, whereas its "opponent" – the generator, wants to confound the generated data with real data.

The first term on the right side represents the log-probability that the discriminator correctly predicts the real data, and the second term represents the log-probability that discriminator correctly predicts the generated data. A successful training process should lead to the improvement of both generator and discriminator, such that the generator will eventually produce indistinguishable samples from the original data set. The input of the generator network are vectors from the latent space, which can be initialized *via* a Gaussian noise function. It should be noted that Fig. 3b is an unconditional GAN architecture, where we don't apply constraints for the input space. If we want to generate samples with certain requirements, a conditional GAN architecture can be adopted.

The emergence of GANs has sparked instantaneous popularity in the computer vision (CV) and natural language processing (NLP) community, where GANs demonstrated the strong capability in image editing,[52] audio syntheses,[53] and domain adaptation.[54] Naturally, researchers have been actively trying to incorporate GANs in material discovery, which is typically an inverse design problem, *i.e.*, search materials with desired properties. Kim *et al.* used GANs to design zeolite structures that have sufficient methane accessibility.[55] They encoded the lattice positions of silicon atoms, oxygen atoms and methane potential energy into a tensor as the input for GANs. After training the network with more than 30k zeolite structures, the GAN were able to produce 121 candidates with a user-desired range of 4 kJ mol^{-1} methane heat of adsorption. Hiraide *et al.* applied GAN to investigate the relationship between structure and Young's modulus of block copolymers.[56] They collected 50 experimental images of block copolymers and augmented the dataset *via* performing operations like rotation, translation, and inversion. After training, the GANs were able to generate promising copolymer structures based on the target Young's modulus, which corresponded to a searching process in the latent space. Besides providing insights for material design, GANs were also able to facilitate computational modelling process. Yang *et al.* applied conditional GANs to predict complex stress and strain fields in composite materials.[57] They established a database of 2k cases *via* finite element method (FEM). For each case, the stress and strain field are calculated based on a 2D pattern consisting of soft units and brittle units that have linear plasticity and strain hardening. Subsequently, the 2D patterns were fed to the generator network as constraints and the strain and stress field were fed to the discriminator network. Although the 2D patterns were a primitive representation of composite materials, the proposed method exhibited excellent predicting accuracy and computational efficiency. Stieffenhofer *et al.* developed a GAN approach to reverse-map coarse-grained (CG) structures to their atomistic resolution.[58] To prepare the database for training and testing, atomistic and CG structures were obtained in MD simulations and this "fine-to-coarse" mapping is regarded as the ground truth. Polystyrene was employed as an example for evaluating the performance of this back mapping approach. Giving the CG snapshot as the conditional input for GAN, the as-trained network successfully captured structural and energetic properties of the polystyrene system. Remarkably, the GAN was able to

recover the equilibrated structure at different temperatures giving the CG snapshots as the conditional variable.

2.2.3 Variational autoencoders (VAE). Variational autoencoders (VAE) are a generative model with continuous latent variables and is a modification of an autoencoder network. VAEs consist of two different parts: an encoder network and a decoder network. As shown in Fig. 3c, the encoder NN will convert input data to a lower dimensional space, *i.e.*, the latent space. The decoder NN will further reconstruct or generate new data from the latent space. Different from a plain autoencoder network, VAEs require regularization in its latent space so that the information is encoded into a meaningful and continuous distribution with a mean of μ and a variance of σ^2, which endows VAEs with the ability to generate new data points *via* sampling from this distribution. The objective for training a VAE model is to maximize the variational lower bound (VLB):[59]

$$\mathscr{L}_{\theta,\phi}(x) = \mathbb{E}_{z \sim q_\phi(z|x)}\left[\log p_\theta(x|z)\right] - D_{\text{KL}}\left(q_\phi(z|x)\|p_\theta(z)\right) \quad (3)$$

Here, x is the observation, z is the hidden variable in the latent space; $p_\theta(z)$ denotes the prior distribution for z, $q_\phi(z|x)$ describes the variational posterior distribution, $p_\theta(x|z)$ is the likelihood during the generative process. The first term represents the expected reconstruction error, and it reflects how well the model reconstructs an observation from a sample from the variational posterior. The second term is the Kullback–Leibler (KL) divergence between distribution $q_\phi(z|x)$ and distribution $p_\theta(z)$. It acts as a regularizer and pushes the variational posterior towards the prior. During training, a random noise variable, ε is induced to the latent space to allow backpropagation of the NN. This process is called the reparameterization trick.[60]

Like GAN, VAE can be used for inverse design of materials. In this case, a property estimation model can be incorporated to the latent space of VAEs to allow for a direct search of desired materials.[61] Attempts have been made for areas such as generating biopolymer with desired affinities[62] and polymers with certain band gap.[63] Yao *et al.* built a material-discovery platform empowered by a supramolecular VAE, which allows the design of metal–organic frameworks (MOFs) with desirable properties.[64] MOFs are reticular frameworks that are composed of organic ligands and metal ions. The authors proposed a graph-based method to efficiently represent the complex structures of MOFs: molecular fragments, multi-connected metal or organic nodes, and topologies are encoded in a tuple. To achieve property prediction, the authors added a property component in the decoder part using labelled data and the tuples were jointly trained to organize the latent space around the properties of interest. After training and optimization, the VAE was able to predict MOF candidates from the latent space with superior gas separation capability, which was confirmed *via* Monte Carlo simulations. Beyond material searching and prediction, VAE can also be applied to material modelling due to its ability to learn compressed representations. Wang *et al.* constructed a VAE framework that could bridge fully atomistic models to coarse-grained models.[65] The input of VAE were atomistic trajectories of individual gas-phase molecules, which were compressed into the CG coordinates that can be treated as latent variables. The output of VAE was reconstructed atomistic coordinates from the latent space. To tune the information learned in the latent space, the authors employed a force regularizer (a regularization term derived from CG force) during training. This regularization will help to obtain a CG free-energy surface, which can be used to simulate systems with a larger spatial and temporal scale.

2.2.4 Recurrent neural networks (RNN). Recurrent Neural Networks (RNN), a class of artificial neural networks, was developed to tailor data that is temporal in nature.[66] The temporal data could naturally be treated in a recurrent fashion; with individual data points, from the temporal dataset, passed sequentially as the input to the recurrent cell. The architecture gained traction in machine translation[67] and speech recognition tasks[68] in the field of natural language processing (NLP).

In the domain of chemistry informatics, there are numerous proposed RNN architectures for many applications ranging from peptide design[67] and drug discovery[69] due to the sequential nature of interpreting peptides as sequences and/or utilizing simplified molecular-input line-entry system (SMILES) representations as sequences. Likewise, in the field of polymer informatics, the 1-D SMILES representation of polymers can be treated as sequential data. Fig. 3d exhibited the architecture of an RNN, and it can be formalized as shown in the equation below:

$$h_t = \sigma(W^{(hh)}h_{t-1} + W^{(hx)}x_t) \quad (4)$$

Here, h_t is the hidden state at time t, σ is the nonlinearity activation, x_t is the input of SMILES token at time t, h_{t-1} is the hidden state output at the prior time step, W^{hh} and W^{hx} are learnable weight matrix. The hidden state, h_t is updated in a recurrent fashion, till the end of the SMILES sequence. The output of the hidden state could be passed on for the supervised learning task, or the hidden state could be formulated with a RNN decoder for unsupervised learning tasks.

In prior work in polymer informatics, Nazarova *et al.* used RNN to predict the dielectric properties of polymers after converting the SMILES representation into the binary representation or American standard code for information interchange (ASCII) representation.[70] Ma *et al.* developed the PI1M dataset,[71] currently the largest available benchmark dataset of approximately 1 million polymers SMILES, by utilizing an RNN architecture to generate syntactically valid polymer-SMILES. The generative modelling task generated new tokens by conditioning on previous subcomponents in the SMILES sequence. Vandans *et al.* used RNN to identify the knot types of polymer conformations.[72] Other input representations, apart from SMILES, for the NN architectures have also been studied with data collected from MD simulations. Andrews *et al.* studied the performance of RNN and their variants on the behavior of energetic properties of a liquid solution containing an aggregation of polymer-lipid macromolecules in an organic solvent.[73] The NNs were trained on potential energies time series of DSPE-PEG (1,2-distearoyl-*sn-glycero*-3-phosphoethanolamine-*N*-(poly-ethylene glycol)$_n$amine) aggregates solvated in ethyl acetate developed through MD simulations. Semine *et al.* used LSTM,

a variant of RNN, to predict the optical spectra using coarse-grained models.[74] The RNN input consisted of a vector of 29 intermonomer dihedral angles; and the output pair being the excited energy relative to the preceding state $(j - 1)^{th}$ state i.e. $(E_j - E_{j-1})$.

Although RNN is widely used in cheminformatics, the potential usage of RNN and its respective variants, gated recurrent unit (GRU) and long short-term memory (LSTM), are lacking due to the limited data available in the domain of polymer informatics. More recent work uses transformers to learn meaningful contextual representations from the polymer-SMILES.

2.2.5 Transformers. Recurrent architectures of GRU, LSTM, and RNN involve generating the current hidden state, h_t, by considering prior hidden states, h_{t-1}. This recursively occurs until the end of the SMILES sequence. However, this sequential approach results in memory constraints due to sequential computation of each hidden state h_t, with respect to the current token.

To solve this problem, the transformer architecture was proposed in 2017 by Vaswani et al.[75] As shown in Fig. 2e, this architecture introduced the attentional mechanism, which helped the model to capture long-range dependencies effectively, which can be challenging for RNNs and CNNs. The transformers used multi-head attention to determine the attention of each token in parallel, with respect to remaining tokens in the SMILES representations. Furthermore, given the challenges of collecting labeled data in cheminformatics and polymer informatics, transformers offer the flexibility of learning representation from large scale unlabeled SMILES data.

Various transformer models such as bidirectional encoder representations from transformers (BERT),[76] robustly optimized BERT-pretraining approach (RoBERTa),[77] and bidirectional auto-regressive transformers (BART)[78] have been developed as effective methods for pre-training on unlabeled data and fine tuning on downstream task performance. In cheminformatics, various transformer architectures have been used for improvising the downstream task performance. Chemformer[79] utilized the BART model for sequence-to-sequence and discriminative cheminformatics tasks. The BART architecture utilized the transformer encoder and decoder. The encoder is provided with the Masked SMILES token, and the decoder is provided with the encoder SMILES sequences that are right shifted. Thus, the output of the decoder produces a distribution over the SMILES vocabulary. ChemBERTa utilized the RoBERTa transformer architecture for masked language modeling (MLM).[80] The authors evaluated the effect of pre-training transformers by replacing SMILES with self-referencing embedded strings (SELFIES) representation. The authors also studied different tokenization strategies of Byte-Pair Encoder and the customer SMILES tokenizer as input to the RoBERTa architecture. The results from the paper highlighted how increasing pre-training data set size for the unsupervised learning task improved the downstream task performance.

Whilst recent trends have seen transformers being utilized in cheminformatics, not until very recently were transformers applied in the domain of polymer informatics. TransPolymer pretrained the PI1M database on the RoBERTa transformer architecture for MLM.[81] The inference or downstream task resulted in the ability to predict various polymer properties, including polymer conductivity, band gap, dielectric constant, refractive index, and power efficiency. PolyBERT used 13 000 synthesized polymers and the breaking retrosynthetically interesting chemical substructures (BRICS) composition to generate 100 million hypothetical polymers.[82] These polymers-SMILES were then trained on the BERT architecture and the resulting embeddings from the self-attention bidirectional transformer encoder were fed to the downstream task performance. The inference tasks were based on polymer thermal, thermodynamic, electronic, optical, mechanical, and permeability properties.

2.2.6 Gaussian processes. Gaussian processes (GPs) are a machine learning method and can be applied to solve regression, classification, and clustering problems.[83] A GP is a collection of random variables, such that any finite number of the variables have a joint Gaussian distribution.[84] It can be denoted as follows:

$$f(x) \sim \mathcal{GP}(m(x), k(x, x')) \tag{5}$$

where $f(x)$ is a real process, $m(x)$ is the mean function and $k(x,x')$ is called the covariance function or kernel function. GPs perform very well for regression problems with small training data sizes. For a regression task, the joint Gaussian distribution is modeled via computing the covariance matrix. The goal is to model the prediction at test points, which is essentially the joint distribution conditioned on the training data and testing input. Therefore, the selection of a proper kernel, k, and the tuning of kernel parameters are vital for a GP. There are multiple kernel functions available, such as radial basis function (RBF) kernel, exponential kernel, sigmoid kernel, periodic kernel, and linear kernel. A good kernel and corresponding parameters should lead to low error in the validation dataset. Fig. 3f depicts how a predicted function is generated from GP based on the training data points. As indicated in the shaded area, the GP also provides additional information about the uncertainty for the predicted function.

GPs are predominantly used for regression tasks in a supervised manner for material predicting and screening tasks.[85–87] Chen et al. employed GPs with an RBF kernel to construct frequency-dependent dielectric models for polymer materials.[88] They utilized a database containing 1210 dielectric constant values measured at different frequencies for 738 polymers. A hierarchical feature fingerprint is used to capture the polymer structure. Following by a feature engineering process, each polymer is converted to a unique 412-dimensional feature vector. The authors then trained a GP regression model that can predict the dielectric constants at different frequencies for unseen polymers. Lopez et al. utilized GP regression to calibrate computational results to experimental data.[89] Since traditional models perform poorly in predicting the performance of non-fullerene acceptor devices, there is a need to predict the molecular orbital energies more accurately. The authors used

a training dataset that is composed of the highest occupied molecular orbital (HOMO) and the lowest unoccupied molecular orbital (LUMO) energies of 94 molecules. With Morgan fingerprints as molecular representation,[90] GP regression with a squared exponential kernel was employed to correct the HOMO and LUMO energies from theoretical calculation. The regression model was further used to help select candidates from 51 000 molecules. Ma *et al.* employed GP regression in a transfer learning scenario to study polymer dynamics.[91] They used GP regression to learn the memory function of a CG model, which played a critical role in reproducing the entire dynamics for the CG modeling. The GP regression established the relationship between the time domain, the parameter space, and the memory function. The CG model developed using the as-trained memory function was able to transfer across a range of parameters and reproduce the dynamic properties of the underlying atomistic systems.

2.2.7 Support vector machines (SVM). Support Vector Machine (SVM) is a classifier that finds the maximum margin separating hyperplane among data points.[92] As shown in Fig. 3g, the data belong to two different classes. SVM algorithm establishes a plane that separates the data with the largest margin, which is achieved by minimizing the loss function. This hyperplane maximizes the SVM's ability to predict correct labels for unseen examples. Without loss of generality, the mathematical form of SVM can be written as:

$$\min_{w} \frac{1}{n} \sum_{i=1}^{n} \max\left[1 - y_i\left(w^{\mathrm{T}} x_i\right), 0\right] + \lambda r(\omega) \tag{6}$$

where the first term is called the hinge-loss that is related to the distance of each data point to the plane, and the second term is a regularization term. Beyond serving as a linear classifier, SVM can also separate data that are not linearly separable *via* introducing kernel functions. Here, a kernel function helps to project low-dimensional data to a high dimensional space, where it is possible to use a high dimensional hyperplane to separate data points. The kernel functions enable SVM to create complex decision boundaries. Although SVM is initially designed for classifying tasks, it can also perform regression.[93] In this case, the hyperplane becomes the fitting results of data points.

Due to its simple architecture and relatively low computational cost, SVM has been applied as one of the most common ML algorithms. Moreover, SVM is frequently used to benchmark NNs.[94,95] Higuchi *et al.* employed SVM to predict the glass transition temperatures of polymers.[96] They prepared a database consisting of 389 T_g values and used *in silico* design and data analysis (ISIDA) descriptors to represent polymer fragments. SVM regression was performed to construct models for linear homo/heteropolymers and crosslinked polymers. Ziaee *et al.* adopted a modified SVM algorithm (least square SVM) to predict the solubility of CO_2 under different temperatures and pressures in various polymers.[97] They compared the performance of several algorithms, such as NN, using the same data set. The SVM model based on an RBF kernel showed the highest predictive accuracy.

2.3 Choice of optimization method

2.3.1 Bayesian optimization (BO). Bayesian optimization (BO) is an approach to optimize expensive objective functions, which commonly builds a surrogate for the objective and quantifies the uncertainty in that surrogate using a GP regression, then adopts an acquisition function defined from this surrogate to decide the next possible sample.[98] Note that the surrogate model does not necessarily have to be GP regression: most ML regression models, *e.g.*, NNs, and kernels can also replace the GP regression for the design space evaluation. The core idea of BO is to explore the design spaces by reconstructing a surrogate model with Bayesian statistics. In a general materials design case, suppose there is a mapping from the representation of the materials to their targeted properties: $X \rightarrow y$, where $X \in \mathbb{R}^n$, *i.e.*, the design variables lie in an n-dimensional space, and $y \in \mathbb{R}$ says the output is projected as a constant(s) representing the materials' properties, *e.g.*, thermal conductivity, toughness, strength. We suppose the general mapping can be represented as $y = f(X)$. In GP regression, one can create a surrogate model for such a map. The model is updated by finding the new observation from $f(X)$'s condition distribution using Bayes' rule. More superficially, the new observation is determined from a prior-induced posterior, namely the acquisition function: $A \rightarrow \mathbb{R}^+$, determines the point in X to be evaluated through the proxy optimization:[99]

$$X_{\mathrm{best}} = \arg \max_{X \in \mathbb{R}^n} A(X) \tag{7}$$

In most materials design scenarios, the acquisition function is of less importance, where most studies employed the expected improvement and/or upper (lower) confidence bound.[100–103] However, the evaluation of the objective, *i.e.* the mapping $X \rightarrow y$, is of key interest in most cases applying BO for materials design. Fig. 4a showed the workflow of BO performing closed-loop optimization with alternating inference and planning stages *via* different surrogate models.[104]

BO is widely applied in materials design and optimization for two reasons: (1) both experiments and the digital twin-based simulation can all be considered as black-box function representations. (2) Both numerical simulations and real-world experiments are either time-consuming or expensive, hence tailoring ad hoc structures or chemical components is inefficient for designing materials with novel applications. By actively searching and exploiting posterior points based on Bayesian statistics, surrogate models can be constructed for exploring the properties of the targeted material. For example, by starting from sparse datasets of polymer measurements, Kim *et al.* discovered polymers possessing high glass transition temperatures with such active-learning strategies.[105] By exploiting *in silico* data of covalent organic frameworks (COF),[106] Deshwal *et al.* demonstrated that designing nanoporous materials using the BO framework can greatly reduce computational resources,[107] and was more efficient than evolutionary and one-shot supervised machine learning approaches. Moreover, Diwale *et al.* presented an augmented BO method to overcome the noise issues in either experiments or simulations.[102]
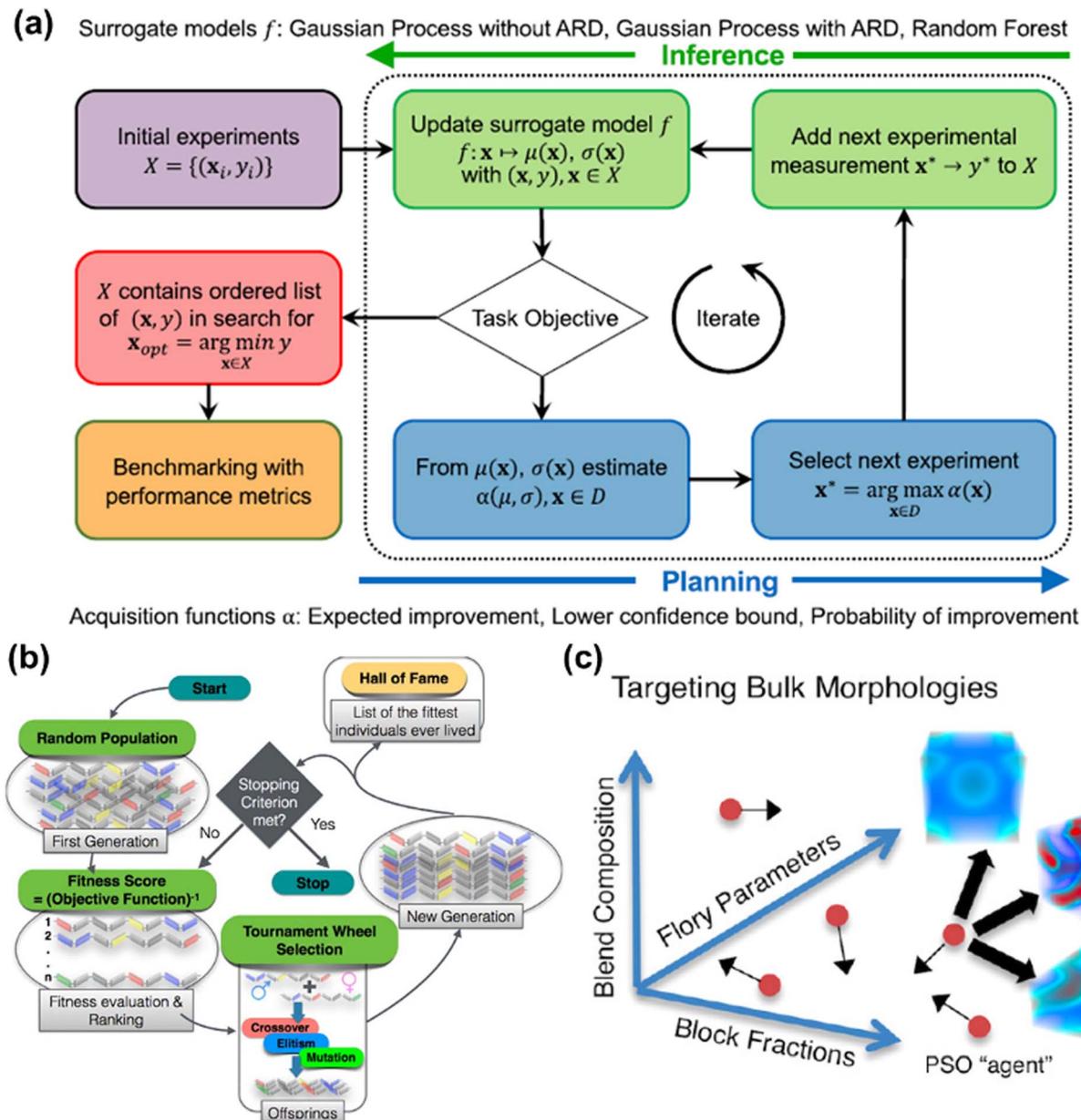
Fig. 4 (a) The flow diagram represents the Bayesian optimization for obtaining the optimal *via* constructing the surrogate model. Image was adapted with permission from ref. 104. (b) A schematic process breakdown of designing polymers with genetic algorithm. Different polymeric compositions are illustrated in different colors of chromosomes. Image was adapted with permission from ref. 128. (c) A cartoon schematic of exploring the design space to approximate the optimum using PSO. Image was adapted with permission from ref. 138.

Besides applications in soft nanomaterials, BO has also been extensively applied in energy storage materials,[100] microstructures of nanomechanical resonators,[108] and alloy design using multi-fidelity approaches.[109,110] From the optimization process perspective, Nakayama *et al.* surveyed the use of acquisition functions and initial values in the BO materials synthesis as a simplified 1D case.[111] Bellamy *et al.* used batch BO to explore a large database for use in drug design.[112] Specifically for the design of polymers, Li *et al.* constructed ML surrogates for experiments and applied BO to propose short fiber polymer designs.[113] Gao *et al.* also used an ML-based surrogate for the objective evaluation of BO for the design of polymeric

membranes.[114] The ML model was trained on a map between the molecular fingerprint to targeted properties. Importantly, Wang *et al.* employed CGMD simulations assisted ML for objective screening with BO for the design of solid polymer electrolytes of high lithium conductivity.[115] In summary, BO has been extensively applied in inverse materials and structural design with targeted properties, mostly employing simulation and using BO to resolve and explore the large design space for more efficient design processing.

2.3.2 Genetic algorithm (GA). Genetic algorithms (GA) are evolution-inspired computational models that use selection and recombination operators to generate new sample points in

a search space for optimizing functions.[116] GA approaches the optimization process by constructing a set of chromosomes to mimic genetic representation. Here, the chromosomes can be represented as:

$$C = [C_1, C_2, \ldots, C_n] \tag{8}$$

where C_i can be interpreted as the data representation of different materials. The group of chromosome sets is then identified as population. These components of the chromosomes within the population can then switch values, which is identified as mutation. The mutated population can reproduce the next population generation through switching chromosomal components, known as crossover. Emulating nature, the "quality" of the genes can be represented *via* their fitness, which are calculated from the crossover chromosomes. Based on the new fitness, GA selects the new population to continue the prementioned processes iteratively for a pre-defined number of generations. Depending on the specific problems, the fitness calculation can vary between different data representations. For any general materials design problems, we may denote the input space as $\mathbb{R}^n$, and the projected output lies in $\mathbb{R}$. The GA-identified fitness resides in the $\mathbb{R}$ space, which we may denote as $\mathcal{F}$. During the selection process, assuming a positive fitness function, the probability of selecting a specific chromosome C_m can be written as:[117]

$$P(C_m) = \left\| \frac{\mathcal{F}(C_m)}{\sum\limits_{i=1}^{n} \mathcal{F}(C_i)} \right\| \tag{9}$$

Fig. 4b demonstrated the steps involved in GA for polymer design. Taking designing soft polyelectrolytes for high electrical conductivity as a thought experiment: the input could be word embedding polymer representations from SMILES,[118] molecular simulation atomic coordinates, or images representing the molecules. The output could be the electrical conductivity as a constant. The simulation can then be represented as a map $\mathcal{M} : \mathbb{R}^n \rightarrow \mathbb{R}$. Under this scenario, the GA tries to maximize the constant in output space and take the input space as chromosomes. Through constructing populations, *i.e.*, running many simulations to generate a set of $\mathcal{M}$; crossover and mutate the chromosome; calculate the corresponding $\mathcal{F}$; and selecting new population for the new loops, the optimal polyelectrolyte can then be selected. Similar strategies have been widely applied in polymer design. Meenakshisundaram *et al.* designed copolymer compatibilizers from MD simulations and GA.[119] Kim *et al.* adopted GP regression to build up surrogate models that map the polymer fingerprints to targeted properties.[120] They used such surrogates for faster evaluation of fitness. Coupling GP regression and GA, they filter polymers with high glass transition temperatures and high bandgaps through a multi-objective approach. Similarly, the same research group used GA with five different ML surrogate models for targeted properties to design polymers for energy storage.[121]

The same group developed a series of GA-enabled polymeric design frameworks. Early GA studies in disordered materials

can be traced back to the 90s,[122] where GA was used in minimizing the energy in MD simulations. GA were used more broadly in materials science in the 2000s. Kim *et al.* applied GA to search for alloy semiconductors with target band structure properties.[123] Similarly, Dudiy and Zunger used GA to search for random structures of semiconductor alloys.[124] At the same time, contributions to applying GA for polymer design emerged. Roy *et al.* leveraged NNs to create surrogate models that map polymer material representations to their properties.[125] They then encode such NNs as fitness functions for GA for optimal polymer design coupled with Markov state modeling techniques. Similar strategies were widely adopted to design monomers.[117] Manos *et al.* use GA coupled with simplified multi-objective fitness functions to design single-mode polymer optical fibers.[126] Similar strategies have also been applied for polymer filtration design optimization.[127] Ramprasad and coworkers contributed much to the recent development of GA for polymer informatics. The group adopted the strategy of evolutionary algorithms to predict polymeric crystal structures back in 2014,[103] then proposed an *ab initio* polymeric properties database and applied GA as a prototype study for polymer design in 2016.[128] Thenceforth, the group developed a series of works combining ML and GA for polymer design.

2.3.3 Particle swarm optimization (PSO). Particle swarm optimization (PSO) is a population-based optimization method inspired by the group behavior of animals that is also initiated with random solutions to search for optimum by updating generations like other evolutionary algorithms.[129] Similar to GA, the algorithm is initialized by a set of populations, as particles, striving to approach the global optimal. Suppose there are p initial particles, and the position of particle i is denoted as $X^i(t) = [X_1^i(t), X_2^i(t), \ldots, X_n^i(t)]$, where t is the iterations (or steps); and n is the dimensions of the design space. The velocity of each particle can be written as $V^i(t) = [V_1^i(t), V_2^i(t), \ldots, V_n^i(t)]$. We can hence write the update of the particles' positions and velocities:

$$X^i(t + 1) = X^i(t) + V^i(t + 1) \tag{10.1}$$

$$V^i(t + 1) = \omega V^i(t) + c_1 \mathcal{R}_1 (\text{pbest}^i - X^i(t)) + c_2 \mathcal{R}_2 (\text{gbest}^i - X^i(t)) \tag{10.2}$$

where c_1 and c_2 are parameters given in the PSO algorithm. pbest^i is the position that gives the best value ever explored by particle i, gbest^i is the best value that explored by all the particles in the swarm.[130,131] The algorithm explores the design space *via* the updated motion of the particles for the optimization goal. Fig. 4c provides a visual presentation of how the particles search in the design space for block copolymers. Recall the previous materials design example: different particles X^i can here be interpreted as different combinations of polymeric chains; the design space can be viewed as the mapping from different polymers to their corresponding targeted properties, and PSO uses particles to explore this design space through updating from their previous locations and velocities. One expects these particles to be clustered around the global optimal, *e.g.*, the maximal electrical conductivity.

Early attempts to apply PSO in materials design occurs around the 2010s: Shokooh-Saremi and Magnusson use PSO for the design of optical diffraction gratings and benchmarked with GA.[132] Interestingly, PSO can be employed for the structural prediction of crystals and layered materials.[133,134] More generally, with very similar approaches, PSO has been adopted to design functionally graded materials,[135] gear train,[136] truss-structures,[137] *etc.*

More recently, PSO was applied to design polymers with the help of different polymeric modeling techniques. Khadilkar *et al.* utilized self-consistent field (SCF) theory as a forward prediction engine and coupled SCF with PSO to identify and design block copolymers and copolymer alloys that self-assemble into a targeted structure.[138] Kumar *et al.* employed gradient boosting with decision trees for the forward modeling of poly(2-oxazoline) and applied PSO for inverse modeling as the workflow for efficient polymer predictive design.[139] Both Francisco *et al.* and Soepangkat *et al.* used PSO for carbon fiber reinforced polymer design,[140,141] in which Francisco *et al.* used finite element methods for fitness calculations in PSO and Soepangkat *et al.* trained a NN with experimental data as a surrogate for the physical responses in fitness evaluations. For the easier application of PSO in the design of novel functional soft materials, *e.g.*, block copolymers, Case *et al.* created an open-source platform with PSO and existed open-source SCF theory software for the inverse design of block copolymers.[142] Using the strategy of coupling PSO and SCF, Tsai and Fredrickson presented a case study of designing globally stable and low-lying metastable meso-phases of block copolymers.[143]

2.4 Case study

In the preceding sections, we have mentioned a series of ML algorithms and optimization methods and how they can be applied to broad topics for materials design and polymer informatics. These topics demonstrate the effectiveness of data-driven approach. In this section, we delve into specific case studies, focusing on the practical application of these algorithms to SPE systems with experimental data.

Back in 2011, feed forward NN was applied to fit the ionic conductivity data obtained *via* experiments.[144] Ibrahim *et al.* measured the conductivity of PEO, $LiPF_6$, ethylene carbonate and carbon nanotubes mixtures under different temperatures. During training, the chemical compositions and temperatures were used as inputs and ionic conductivities as outputs. The simple NN was able to predict the ionic conductivity of such a system well, as the predicted value can be further validated with new experiments.

Hatakeyama-Sato *et al.* employed ML methods to explore superionic glass-type SPEs with aromatic structures. They constructed a database including 10^4 entries about ionic conductivity. First, GNN was utilized to truncate molecular descriptors and extract useful features.[34] The NN is pretrained on a database of randomly generated *de novo* polymers and monomeric compounds. The goal of this pretraining is to predict 2000 molecular descriptors from these compounds using only 32-dimensional vectors. This vector was then used to represent the feature of each compound for further ML processes. Subsequently, GP was used for establishing the relationship between chemical features and ionic conductivity. GP was able to output conductivity values along with confidence intervals. Combining GNN and GP, the authors successfully yielded glass-type polymer complexes with high conductivity that was later validated *via* experiments.

Bradford *et al.* built a chemistry-informed ML model that could predict SPE ionic conductivity based on the electrolyte and composition.[145] They gathered data set of SPE ionic conductivity values from 217 experimental publications. They adopted a message passing NN, which is a special type of GNN, to learn optimal representations of the molecular components. The input of the NN took vectorized SPE features including polymer structure, salt structure, polymer molecular weight, salt concentration and temperature. The authors encoded the Arrhenius equation, which describes temperature dependence of ionic conductivity, into the readout layer of the NN and found that this chemically informed layer would increase prediction accuracy of the NN. After training the NN, they used the model to screen over 20 000 potential SPEs composed of commonly used lithium salts with synthetically accessible polymers and identified promising candidates. The predicted ionic conductivity exhibited good agreement with two types of in-house synthesized polymers. Furthermore, they extended their predictions to encompass various anions within PEO and poly(trimethylene carbonate), showcasing the model's effectiveness in identifying descriptors for solid polymer electrolyte (SPE) ionic conductivity.

3 ML aided polymer computation

3.1 Density functional theory (DFT)

Density Functional Theory (DFT) is an *ab initio* quantum mechanical (QM) method widely used to elucidate material properties, such as electronic band structures, vibrational frequencies, and magnetic configuration, to name a few, through various codes or algorithms. Instead of solving the many-body Schrödinger equation, the reformulated Kohn–Sham equation[146] in DFT gives self-consistent solutions by recasting the multi-electron interactions as a single electron system with the approximate exchange–correlation functional, as shown in the following:

$$\left[-\frac{\hbar}{2m}\nabla^2 + V_{ext}(r) + V_H(r) + V_{XC}(r) \right]\psi_i(r) = \varepsilon_i\psi_i(r) \quad (11)$$

where $-\frac{\hbar}{2m}\nabla^2$ is the kinetic energy operator for electron kinetic energies, $V_{ext}(r)$ is the Coulomb potential for electron–nuclei interactions, $V_H(r)$ is the Hartree potential describing the Coulomb potential from the electron charge density, and $V_{XC}(r)$ is the exchange–correlation functional with all QM effects. Commonly used functionals include VWN,[147] PW91,[148] M06-class,[149] ωB97-series,[150] B3LYP,[151,152] *etc.*, belonging to different families—linear-density approximation (LDA), generalized gradient approximations (GGA), meta-GGA, and hyper-GGA,
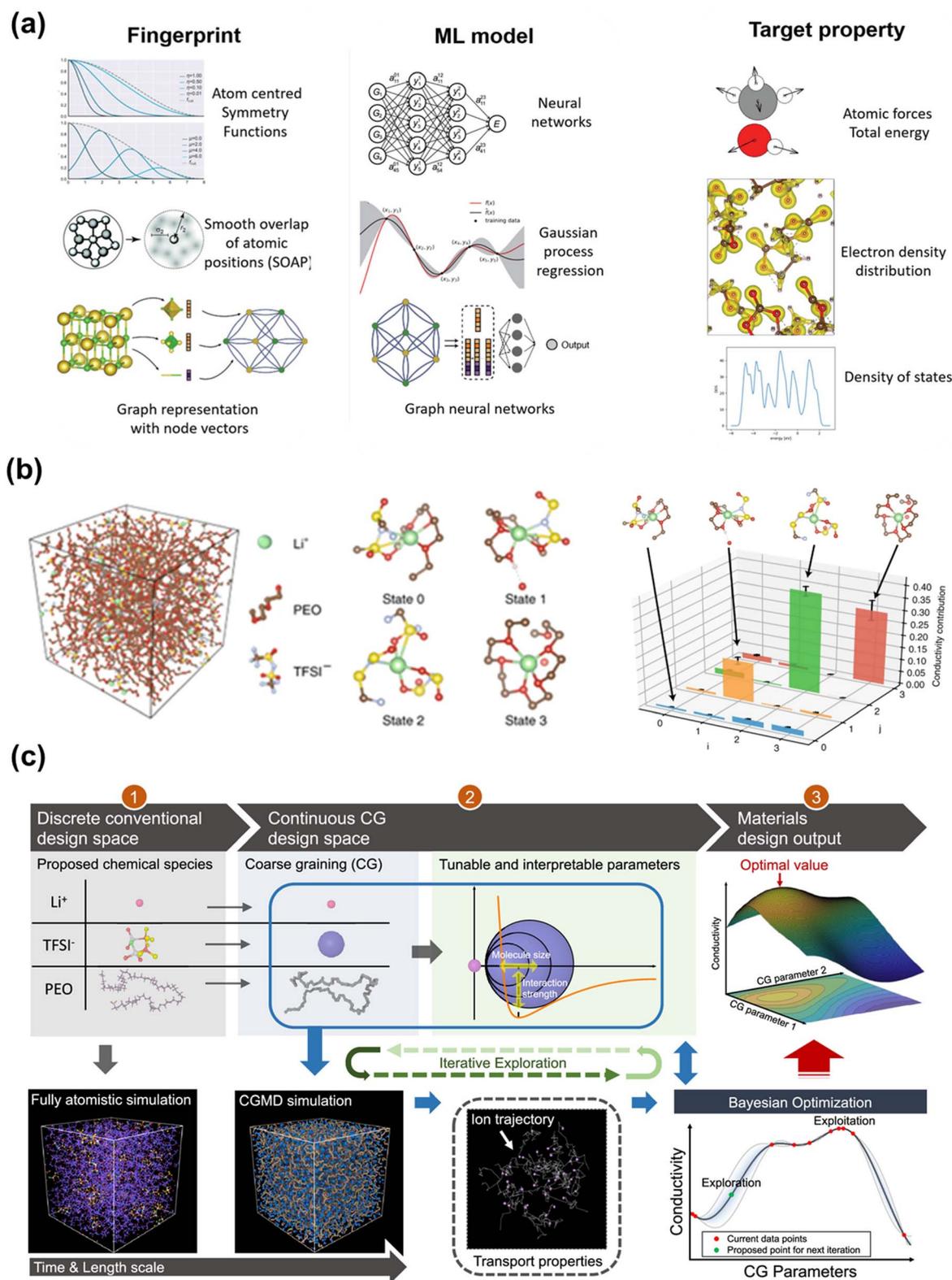
Fig. 5 (a) Some fingerprints, ML models and target properties for constructing MLPs. Image was adapted with permission from ref. 170. (b) An example of using GNN to conduct unsupervised learning on MD trajectories of Li⁺ in a SPE. Image was adapted with permission from ref. 31. (c) The framework of employing CG and BO for design of PEO-based SPEs. Image was adapted with permission from ref. 115.

etc., with their strengths and weakness. Many DFT textbooks and articles have provided valuable insights on selecting functionals and basis sets with examples of applications.[153–155]

In solid polymer electrolytes, DFT can estimate, for example, energy-related changes and local ion–polymer interactions in polymeric matrices for electrochemical stability window and ion migration,[156,157] as well as band gap and molecular orbital for electronic charge transport properties.[158,159] Researchers can take advantage of accuracy and are also eligible for computing various materials in DFT calculations since no external potential or force fields are required as input. Despite this, the time and length scales of the systems for DFT calculations, in general, are small. In contrast, the systems of polymer electrolytes are always large and complex with macromolecular solvents, leading to high computational costs. An efficient way to avoid this side effect is to combine data-driven ML methods discussed in previous sections. ML-aided DFT frameworks were reviewed by Mannodi-Kanakkithodi *et al.* and Schleder *et al.*[160,161] Specifically, fully exploiting the development of the extensive DFT datasets for training ML models shows great potential to enable the design and discovery of novel electrolyte systems containing polymer and lithium or other alkali metal compounds with wide electrochemical stability window, high ionic conductivity, and good thermal and mechanical stability in a fraction of the time.[27,160,162,163] For example, Li *et al.* developed a ML workflow embedded with DFT and GNN to discover promising ionic liquids as additives for SPEs. DFT was employed to calculate the training data of electrochemical stability window based on HOMO/LUMO theory. The authors further verified a subset of selected candidates and measured the performance using experiments.[164] Besides, high-throughput DFT databases for small molecules or compounds have increased considerably in recent years. Examples are the Materials Project[165] **https://materialsproject.org/** containing DFT calculated structures and electronic properties for more than 140 000 materials; AFLOWLIB[166] **aflowlib.org/** comprising phase diagrams, electronic structure, and magnetic properties of 150 000 alloys and 13 000 inorganic compounds; the Open Quantum Materials Database (OQMD)[167] **https://oqmd.org/** consisting of nearly 300 000 DFT total energy calculations of inorganic crystal structure; and the Organic Materials Database (OMDB)[168] **https://omdb.mathub.io/** with thousands of Kohn–Sham electronic band structures. Many other such databases were reviewed recently.[161,169] In addition to the existing databases, ML models can be built upon freshly generated data. The size of the dataset depends on the complexity of ML models and algorithms, the number of features and input diversity, the expected prediction error, and others, but in general, the more, the better. Different sizes of the generated datasets have been used in various DFT+ML studies, ranging from 10^2 to 10^5 samples,[160] but are commonly relatively small due to the high computational costs, which can dominate most of the time in a project.

To take advantage of the accuracy of DFT calculations but circumvent the limitations of simulation scales, ML potentials (MLPs) are used to bridge the gap between QM and classical force fields. Fig. 5a manifested that ML models can map from

a three-dimensional configuration of atoms to energies and forces using fingerprints such as atom centered symmetry functions.[170] This will enable large-scale atomic simulations with dynamic properties and fill in the blanks whenever there are no empirical force fields available, which is beneficial for solid polymer electrolyte systems. Compared to *ab initio* MD (AIMD) or Born–Oppenheimer MD that extract potential energy directly from DFT or other QM methods at every step,[171] MLPs interpolate *ab initio* calculations by training the *ab initio* or DFT dataset and thus extend the system size and time scale in MD simulations. For example, Musaelian *et al.* recently introduced a deep NN interatomic potential architecture to achieve simultaneously accurate and computationally efficient parameterization of PES. In one of their testing cases, the authors simulated the Li-ion migration in a Li_3PO_4 electrolyte. Compared to AIMD, a mean absolute error in energies of 1.7 meV per atom was obtained for the proposed MLP. The authors further demonstrated the superior scaling ability of this method by running a system containing 421 824 atoms on multiple GPUs.[172] Fu *et al.* benchmarked a collection of state-of-the-art MLPs under different practical scenarios. Apart from force and energy prediction errors, the authors suggested other metrics to evaluate MLPs such as radial distribution function (RDF) and diffusivity coefficient for LiPS dataset.[173] A more comprehensive review of recent advances in MLPs was given elsewhere.[174–176] Generally, MLPs require an input of descriptors transformed from the atomic coordinates and output the potential energy mapped from an ML model. A descriptor needs to be invariant under translation, rotation, or the permutation of atoms, and independent of the system size.[177,178] One of the most widely used structural descriptors is a set of symmetry functions of each atom initially developed by Behler and Parrinello, which contains radial and angular parts to capture the pair and triplet properties.[177,179] Those symmetry functions reflect the atomic environment that provides a unique description of the atomic positions.[178] Many subsequent models revolved around the improvements to symmetry functions. For example, the ANAKIN-ME (ANI) model[180,181] divide the atomic environment based on atom types to accelerate the sampling of MLP surface; the Charge Equilibration Neural Network Technique (CENT)[182–184] redistribute charge density in the system to environment-dependent atomic electronegativities for considering long-range interaction; and the weighted symmetry functions (wACSF) introduce element-dependent weighting functions to simplify the system with a large number of different chemical elements.[185] Besides symmetry functions, many other input descriptors, including the bispectrum of the neighbor density,[186] Smooth Overlap of Atomic Positions (SOAP),[187] and the Coulomb matrix,[188] are designed in various models, which are detailed in Behler's review.[189,190] In fact, all the descriptors try to keep the invariances or preserve the "symmetries" in a system while including more physical properties.

ML methods leverage purely mathematical structures, and the most popular algorithms for constructing MLPs are NN- and kernel-based methods. In NN-based MLPs, the output of the NN is the total energies of the system by summing each atom's

energy predicted by each fully connected NN through minimizing the loss function containing the energy error[180,184] or, in addition, force error[181,191,192] or even additional stress error[193,194] and charge error[195] between AIMD and MLP simulations. Kernel-based methods, *e.g.*, using GP, provide the best energy estimates by weighted summing of the energies over the reference configurations through kernels. Uncertainty quantification[196] and active learning[197] can be employed to construct the training dataset with the required size and accuracy by enabling automated model correction and prediction ability improvement.[174] Here, we briefly introduce some latest packages and platforms for MLPs. For example, ANI model[180,181] is an NN-based MLP, applying the Behler-Parrinello method[177] to construct NN for organic molecules but with modified symmetry functions to build single-atom atomic environment vectors as a molecular representation. The latest ANI-2x has been trained to seven elements (H, C, N, O, F, Cl, S), making up 90% of drug-like molecules. The open-source implementation of ANI is available in PyTorch.[198,199] **https://github.com/aiqm/torchani** with the accessible dataset.[200] Deep Potential Molecular Dynamics (DPMD) method is another NN-based MLP that can be implemented using the DeePMD-kit package **https://github.com/deepmodeling/deepmd-kit**.[194,201] In DPMD, the input descriptors are the local Cartesian coordinate frame for each atom, thus overcoming the limitations associated with auxiliary quantities in symmetry functions.[194] Other NN-based MLPs include the TensorMol model[191] **https://github.com/jparkhill/TensorMol** that captures long-range electrostatics and the AIMNet model[202] **https://github.com/aiqm/aimnet** that uses atomic feature vectors to record the interactions of neighboring atoms and updates by passing messages through the NN. Besides NN-based MLPs, Gaussian Approximation Potentials (GAP)[186] apply the GP approach to construct MLPs for high-dimensional systems, and SOAP kernel[187] is widely used to train the potential. The code is implemented in the QUIP package[203] **https://github.com/libAtoms/QUIP** with a brief tutorial introduction.[204] Furthermore, the RuNNer Neural Network Energy Representation[177,205] **https://theochemgoettingen.gitlab.io/RuNNer/1.3/** is a Fortran-based framework implementing the latest version of Behler-Parrinello-type high-dimensional NN potentials with the 4G datasets[206] **https://archive.materialscloud.org/record/2020.137**, and Open Knowledgebase of Interatomic Models (OpenKIM)[207] **https://openkim.org** is a repository of interatomic potentials containing various pre-trained MLPs.

Although MLPs have been used to successfully simulate a more extensive system accompanied by continuing developments in algorithms and computing hardware and software, it is still difficult to apply MLPs to systems with many degrees of freedom due to the complexities associated with interpolations. In other words, if a system travels to a new configuration outside the PES constructed by the training dataset, the MLPs may give us inaccurate energy states, which require a broader training dataset that can cover enough points on the PES and needs more computational resources.

3.2 Molecular dynamics (MD) simulations

The Born–Oppenheimer approximation aggregates the effects from electrons surrounding the atomic nuclei and simplifies the QM laws governing the interactions between atoms using the laws of Newtonian mechanics.[176] This approximation reduces the amount of computation needed for a simulation by orders of magnitudes. We have discussed how ML can help to extract classical PES from QM calculations to enable fast and accurate MD simulations. Indeed, MD makes it possible to simulate material systems with atomistic-level details at micrometers in length scale and microseconds in time scale. Therefore, with MD, it is not hard to obtain atomistic trajectories spanning relatively longer time scale compared to QM computations. ML has been applied to analyze such trajectories to extract knowledge about both the energetic and kinetic aspects of the atomistic system.[208] Recently, there also has been efforts to apply ML to learn the mapping between the configuration and the mechanical properties of polymer composites.[209]

3.2.1 ML to construct free energy surfaces. As the compositions and structures of SPEs become increasingly sophisticated, the investigation of ion transport kinetics within SPEs and across SPE-electrode interface are growing in importance.[210–212] While PES describes the potential energy landscape of a system and can be primarily used for structural optimizations of molecules (*e.g.*, the rearrangements between isomers), the free energy surface (FES) includes information of both potential energy and entropy contributions and can be used for assessing kinetics and thermodynamics of bulk molecular systems (*e.g.*, protein folding) at a given temperature.[213,214] Currently, there's ample research opportunities for constructing FES of SPE systems.

An accurate description of the free energy is key to understanding complex systems that have many intrinsic degrees of freedom.[215,216] The relevant configurations of such systems and the transition between them can be captured by reducing the high-dimensional PES to a low-dimensional FES. Concretely, for a large system that contains N atoms, it requires roughly $3N$ degrees of freedom to describe the PES. Yet, we aim to employ collective coordinates with significantly fewer dimensions than $3N$ to encode information.[208] This is particularly helpful for description of the chemical processes and the validation of computational models.[215,217]

Accurate generation of free energies from simulation is an outstanding challenge.[218,219] In practice, free energy is usually computed as discrete data points by probing individual molecular configurations, rather than as a continuous analytic function.[216] Suppose for a molecule with atom positions x in the Cartesian coordinates, a set of collective variables is used to represent the relevant degrees of freedom. In practice, the collective variables are chosen based on chemical or physical intuition such that they encode some important structural information in a molecule such as the length of some critical chemical bond or the backbone dihedral angles of an organic compound.[218,220]

Given an MD trajectory labeled with free energy estimation or the gradient of the free energy, an ML model learns

a function defined on the collective variable space to reconstruct the FES using either the free energy loss or the free energy gradient loss.[208] Kernel methods such as GP regression[221,222] and deep NNs have been used to this end.[216,218,222] The learned model can provide in-depth knowledge of the system such as differences of free energy between different states or even the ensemble averages of certain physical observables.[218]

3.2.2 ML to construct kinetic models. From the kinetic aspect, ML also helps to construct Markov state models (MSM) from MD trajectories to understand the dynamical processes that govern the performance of functional materials for better material design.

ML-based approaches are based on several mathematical achievements. One of the most fundamental results that facilitates the ML practice in this area of study is the Koopman theory. This theory states that there exists a function χ that maps the local configuration of atoms x in MD to a feature space $\chi(x)$ in which the dynamics can be approximated using a linear transition matrix:[31]

$$\chi(x_{t+\tau}) = K^{T}\chi(x_t) \qquad (12)$$

where K is the Koopman operator. In recent years, the VAMP theory provides a powerful tool to measure the consistency between learned singular functions of K and the underlying true ones, which is used constructively when defining the loss function for training purposes.[43,223] Moreover, the atomistic structures of materials, either organic or inorganic, can be understood in a graph theoretic way, because they are mostly defined by particles (nodes) and interactions (edges).[224–227] Therefore, the graph convolutional networks (GCN) have become a natural class of tools to learn the MSM from the MD trajectories. GCN is a direct generalization of convolutional neural networks (CNN) to graph-structured data.[228,229]

In a pioneering work,[31] researchers study the dynamics of lithium ions in solid polymer electrolytes using MSM built by graph convolutional NNs. As shown in Fig. 5b, a four-state MSM identifies three relaxation processes, and the slowest relaxation is shown to involve the transport of a Li-ion into and out of a polyethylene oxide coordinated environment. The authors remark that despite that the relaxation processes of the solid polymer electrolytes have been extensively studied, the machine-learned MSM is still insightful because it provides the exact atomic-scale dynamics related to these relaxations, which can be further related to ionic conductivity.

3.2.3 ML to aid simulation-driven design. ML can also be aggregated with MD simulations to understand the relation between the chemical configuration and the mechanical properties of polymeric composites. The material structure–property mapping can be sampled using a relatively small amount of MD simulations. After sampling, ML can be applied to learn such maps and predict the properties of unseen structures.

For example, optimizing the functionalization of carbon nanotubes (CNT) in the polymer matrix is a possible route to improve the interfacial shear strength in such composites.[230] This is because the functionalization improves the load transfer between the CNT and the matrix, while it also disrupts the

pristine CNT lattice structure that is responsible for the superior properties of the CNT.[231] Therefore, there could be some functionalization state that maximizes the interfacial shearing strength. A recent work uses ML to aid the MD-driven design of carbon nanotube (CNT)–polymer composite.[209] The design variable is the covalent functionalization of the CNT atoms by creating covalent bonds between the polymer and the CNT in the simulations. Pullout tests are performed to sample the mapping between the material design and the critical pullout force. This work uses the Radial Distribution Function (RDF) along with several structural descriptors as the feature representation of the CNT. A CNN trained on the feature space and the observed critical pullout force is shown to have satisfactory accuracy. Such models can be even more powerful if integrated into optimization frameworks to maximize the desired mechanical properties. Another recent work *via* Xie *et al.* developed a multitask GNN to accelerate MD simulation of LiTFSI/SPE systems.[232] The NN is trained on a large number of short, unconverged MD simulations and a small number of long, converged MD simulations. The trained NN is able to reduce errors and make predictions based on short MD simulations. The developed ML model is employed to perform an extensive screening of potential polymer electrolytes. An open dataset from the model was generated for the design of SPEs.

3.3 Coarse-grain (CG) modelling

Various CG models have been employed to construct SPEs. The most well-developed model is Kremer–Grest (K–G) model, which is suitable for studying dynamic,[233] and mechanical properties of polymer melts.[234,235] K–G model describes a polymer chain as a string of hard-sphere beads connected *via* springs. The length and the strength of the springs are related to the Kuhn length and the stiffness of the polymers. The bonded interactions are usually described by the finitely extensible nonlinear elastic (FENE) potential:

$$U^{\text{FENE}} = -\frac{1}{2}KR_0{}^2 \ln\left(1 - \left(\frac{r_{ij}}{R_0}\right)^2\right) + 4\varepsilon_{ij}\left(\left(\frac{\sigma_{ij}}{r_{ij}}\right)^{12} - \left(\frac{\sigma_{ij}}{r_{ij}}\right)^6\right) + \varepsilon_{ij} \qquad (13)$$

The non-bonded interactions are usually described by the 12-6 Lennard-Jones (LJ) potential:

$$U^{\text{LJ}} = 4\varepsilon\left[\left(\frac{\sigma_{ij}}{r_{ij}}\right)^{12} - \left(\frac{\sigma_{ij}}{r_{ij}}\right)^6\right] \qquad (14)$$

The K–G model has been employed to investigate the self-assembly,[235] correlation between microstructure and ionic mobility,[236] electric field effects on the polymer aggregation,[237] *etc.* A variant of K–G bead-spring model was developed by Kumar *et al.*[238] They modeled poly(ethylene oxide) (PEO) and embedded Stockmayer dipoles in each bead that could better capture the local electrostatic interactions between Li-ions and PEO.

An alternative well-known CG model is dissipative particles dynamics (DPD). In the late 1990s, Groot *et al.* developed DPD simulation that provided a new approach to perform large scale MD simulation.[239] Different from the relatively simple LJ non-bonded interaction, the DPD defines three non-bonded inter-action terms for each pair-wise particles within a cut-off distance r_c:

$$f_i = \sum_{j \neq i} \left(F_{ij}^C + F_{ij}^D + F_{ij}^R \right) \tag{15.1}$$

$$F_{ij}^C = \begin{cases} a_{ij}(1 - r_{ij})\hat{r}_{ij} & (r_{ij} \leq r_c) \\ 0 & (r_{ij} > r_c) \end{cases} \tag{15.2}$$

$$F_{ij}^D = -\gamma_w^D(r_{ij})(\hat{r}_{ij} \cdot v_{ij})\hat{r}_{ij} \tag{15.3}$$

$$F_{ij}^R = \sigma_w^R(r_{ij})\theta_{ij}\hat{r}_{ij} \tag{15.4}$$

As shown in the above equations, the total non-bonded force acting on the ith particle equals to the sum of the conservative force F_{ij}^C, the dissipative force F_{ij}^D, and the random force F_{ij}^R. The F_{ij}^C is a soft repulsion force where a_{ij} represents the maximum repulsive interaction between the ith and j^{th} particle. The value of a_{ij} was benchmarked by the compressibility of water,[239] and the a_{ij} for other molecules were mapped onto Flory–Huggins parameters, which can be then derived by the solubility or mixing energy.[240,241] The dissipation constant γ and the noise amplitude σ are correlated by $\sigma = \sqrt{2\gamma k_B T}$. The $w^D(r_{ij})$ and $w^R(r_{ij})$ are functions solely depend on the distance r_{ij}. In the random force equation, θ_{ij} is a random variable obeying Gaussian distribution. Coupling with the smeared charge approximation, DPD model have succeeded in study the electrostatic interaction[242] and the ion conductivity[243] of the poly-electrolyte systems.

It should be noted that both K–G model and DPD model are considered top-down CG approaches, *i.e.*, the explicitly proposed simple potentials are tuned to match macroscopic thermodynamic properties.[244] In contrast, bottom-up CG approaches employ more complex potentials that are parame-terized with information from atomically detailed simulations. Therefore, bottom-up CG can be better at capturing local interactions, such as polarized effect in SPEs, and preserving chemical specificity.[245] There are some recent reviews that have discussed bottom-up CG approaches in more detail.[246,247]

The CG model broadens the temporal and spatial scales of the simulation, but also introduces uncertain CG parameters that are flexibly tunable within a reasonably range. Therefore, Grossman *et al.* exploited the CG parameter space with the help of BO to design a PEO-based SPEs having higher Li-ion conductivity.[115] Fig. 5c illustrates the workflow of incorpo-rating BO with CG for such design process. In their CG model, a Class2 force field and the LJ 12-6 potential were adopted to describe bonding and non-bonding interactions, respectively. Specifically, they designated all CG parameters into three cate-gories: anion-related parameters (anion size, salt concentration, *etc.*), parameters related to the polymer chain (monomer size, *etc.*), parameters related to the secondary structure (molecular

size, *etc.*). Clearly, the CG parameter space is a complex high-dimensional space. Bayesian optimization constructed a continuous function mapping the CG parameter space to a one-dimensional space (Li-ion conductivity). They chose Gaussian process prior to describe the function. Posterior was evaluated based on the prior and the current CG simulation data. The next trial point was determined by an acquisition function, *i.e.*, lower confidence bound modified by the local penalization method. Compared with random search, BO-assisted CG found a design plan to yield higher Li-ion conductivity within shorter iterations.

ML was conventionally employed to predict the CG force field, as the example mentioned above, while a novel idea was proposed to directly predict the dynamics of CG systems.[248] It overcame two challenges: learning-based force field becomes unstable after a long timescale simulation; learning-based force field limits to specific systems. They first learned atom embedding information at the fully atomistic level using an embedding GNN. Subsequently, they coarse grained the system using graph clustering. Finally, the dynamics, *i.e.*, time-integrated acceleration was learned at the CG scale by a dynamics GNN. Using this scheme, just a set of short MD trajectories are needed, which greatly reduces the computa-tional cost. They validated the scheme on two realistic scenarios, polymers in implicit solvent and Li-ion SPEs.

4 Conclusions and outlook

The macroscopic properties of SPEs originate from the intricate interplays among various physical parameters across multiple scales. ML can provide an alternative shortcut to circumvent the challenge of fully understanding those complex mechanisms and establish a surrogate model from input features to output properties. In the above sections, we have reviewed different ML algorithms and their applications to SPE research, ranging from screening, discovery, and optimization of novel SPEs to gener-ating force field. We highlighted how ML algorithms could be incorporated with theory-based modelling techniques and the new framework would improve computation efficiency and scalability. As this area is growing rapidly, there are several emerging challenges that require to be addressed. (i) The open-source databases with extensive and detailed polymer data entries are in pressing demand. Data-driven approaches rely highly on data of good-quality to avoid the so called "garbage in, garbage out" scenario. Although some databases have contrib-uted substantially to building ML models for SPEs, it is yet difficult to directly find properties such as ionic conductivities or electrochemical stability window for a vast majority of poly-mers. Moreover, it would be ideal for databases to include more information about copolymers, branched polymers, crosslinked polymers, and polymer composites since these polymer systems are regarded as crucial strategies for optimizing ionic conduc-tivities and mechanical properties. One way to achieve such goals is to create live databases that are friendly for users to access and edit. Efforts have been made to promote data sharing for both experimentalists and theorists in public repository.[163,249,250] With such repositories, experimentalists are

expected to document accurate experimental data about SPEs such as ionic conductivity, mechanical properties, and morphological information. Meanwhile, computational chemists are expected to modify existing descriptors or design new descriptors that are compatible for more complicated polymer systems that can be beneficial for establishing a more comprehensive database. (ii) Studies about evaluating and comparing the performance of different ML algorithms on certain tasks such as training MLPs are still limited. On the one hand, ML community has developed plenty of algorithms that can be used interchangeably for the same problem with pros and cons, and the evolution of ML algorithms is still at a swift pace. On the other hand, some ML architectures have lots of hyperparameters and can be very flexible. We are hoping that more studies can investigate benchmarks for various ML algorithms across different use cases and report nuances during hyperparameter tuning, which can guide future researchers to build their own ML pipelines. Apparently, having standardized and wildly acknowledged databases will greatly facilitate benchmarking process. Moreover, it is essential for computational chemists to open access to their code for public use, thereby reducing the barriers to implementing ML models. (iii) The ambition towards achieving fully automated SPE development involves the integration of theory-based modeling, machine learning algorithms, and high-throughput experimentation. High-throughput experimentation has been employed in areas such as drug discovery and polymer syntheses.[251,252] Especially for generative models, high-throughput experimentation can quickly validate the accuracy and effectiveness of the results output by the theoretical computation plus ML framework, since the generative models may often come up with samples that are never seen before. Furthermore, high-throughput experimentation can bestow a data-driven approach with improved error tolerance. With high-throughput experimentation, the researchers can not only test the optimal selected by the model, but also test a subset of the candidates that have close scores to the optimal. Once more, a robust partnership between experimentalists and computational chemists remains essential in crafting such workflows. Computational chemists can assist experimentalists in designing experiments and ensure that experiments are efficient, cover a wide parameter space, and provide meaningful data. Concurrently, experimentalists can help computational chemists gain a deep understanding of SPEs to adjust and improve their models. In a nutshell, though still in the early stage, the success of ML in solving a variety of challenges in SPEs indicates the promising potential of this computational and data-driven technique for better SPEs in the future.

Data availability

As this is a Review article, no primary research results, data, software or code have been included.

Conflicts of interest

There are no conflicts to declare.

Acknowledgements

References

1 X. B. Cheng, C. Z. Zhao, Y. X. Yao, H. Liu and Q. Zhang, *Chem*, 2019, **5**, 74–96.

2 M. Li, C. Wang, Z. Chen, K. Xu and J. Lu, *Chem. Rev.*, 2020, **120**, 6783–6819.

3 A. Manthiram, X. Yu and S. Wang, *Nat. Rev. Mater.*, 2017, **2**, 1–16.

4 G. Xi, M. Xiao, S. Wang, D. Han, Y. Li and Y. Meng, *Adv. Funct. Mater.*, 2021, **31**, 1–28.

5 J. Lopez, D. G. Mackanic, Y. Cui and Z. Bao, *Nat. Rev. Mater.*, 2019, **4**, 312–330.

6 L. Fan, S. Wei, S. Li, Q. Li and Y. Lu, *Adv. Energy Mater.*, 2018, **8**, 1–31.

7 X. Yang, J. Luo and X. Sun, *Chem. Soc. Rev.*, 2020, **49**, 2140–2195.

8 Q. Zhao, S. Stalin, C. Z. Zhao and L. A. Archer, *Nat. Rev. Mater.*, 2020, **5**, 229–252.

9 D. Zhou, D. Shanmukaraj, A. Tkacheva, M. Armand and G. Wang, *Chem*, 2019, **5**, 2326–2352.

10 W. Zhou, Z. Wang, Y. Pu, Y. Li, S. Xin, X. Li, J. Chen, J. B. Goodenough, W. Zhou, Y. Pu, J. Chen, Z. Wang, X. Li, Y. Li, S. Xin and B. Goodenough, *Adv. Mater.*, 2019, **31**, 1805574.

11 Q. Wang, H. Wang, J. Wu, M. Zhou, W. Liu and H. Zhou, *Nano Energy*, 2021, **80**, 105516.

12 R. Khurana, J. L. Schaefer, L. A. Archer and G. W. Coates, *J. Am. Chem. Soc.*, 2014, **136**, 7395–7402.

13 C. Monroe and J. Newman, *J. Electrochem. Soc.*, 2005, **152**, A396.

14 D. G. Mackanic, X. Yan, Q. Zhang, N. Matsuhisa, Z. Yu, Y. Jiang, T. Manika, J. Lopez, H. Yan, K. Liu, X. Chen, Y. Cui and Z. Bao, *Nat. Commun.*, 2019, **10**, 1–11.

15 X. Wang, C. Zhang, M. Sawczyk, J. Sun, Q. Yuan, F. Chen, T. C. Mendes, P. C. Howlett, C. Fu, Y. Wang, X. Tan, D. J. Searles, P. Král, C. J. Hawker, A. K. Whittaker and M. Forsyth, *Nat. Mater.*, 2022, **21**, 1057–1065.

16 C. Yang, Q. Wu, W. Xie, X. Zhang, A. Brozena, J. Zheng, M. N. Garaga, B. H. Ko, Y. Mao, S. He, Y. Gao, P. Wang, M. Tyagi, F. Jiao, R. Briber, P. Albertus, C. Wang, S. Greenbaum, Y. Y. Hu, A. Isogai, M. Winter, K. Xu, Y. Qi and L. Hu, *Nature*, 2021, **598**, 590–596.

17 F. Chen, X. Wang, M. Armand and M. Forsyth, *Nat. Mater.*, 2022, **21**, 1175–1182.

18 S. J. Tan, X. X. Zeng, Q. Ma, X. W. Wu and Y. G. Guo, *Electrochem. Energy Rev.*, 2018, **1**, 113–138.

19 E. Umeshbabu, B. Zheng and Y. Yang, *Recent Progress in All-Solid-State Lithium–Sulfur Batteries Using High Li-Ion Conductive Solid Electrolytes*, Springer Singapore, 2019, vol. 2.

20 P. M. Ketkar, K. H. Shen, L. M. Hall and T. H. Epps, *Mol. Syst. Des. Eng.*, 2019, **4**, 223–238.

21 L. Wang, Y. Ye, N. Chen, Y. Huang, L. Li, F. Wu, R. Chen, L. Wang, Y. Ye, N. Chen, Y. Huang, L. Li, F. Wu and R. Chen, *Adv. Funct. Mater.*, 2018, **28**, 1800919.

22 N. S. Schauser, G. A. Kliegle, P. Cooke, R. A. Segalman and R. Seshadri, *Chem. Mater.*, 2021, **33**, 4863–4876.

23 C. Lv, X. Zhou, L. Zhong, C. Yan, M. Srinivasan, Z. W. Seh, C. Liu, H. Pan, S. Li, Y. Wen and Q. Yan, *Adv. Mater.*, 2022, **34**, 1–17.

24 Y. Liu, O. C. Esan, Z. Pan and L. An, *Energy AI*, 2021, **3**, 100049.

25 D. J. Audus, J. J. De Pablo, *ACS Macro Lett.*, 2017, **6**, 1078–1082.

26 X. Zhong, B. Gallagher, S. Liu, B. Kailkhura, A. Hiszpanski and T. Y. J. Han, *npj Comput. Mater.*, 2022, **8**, 1–19.

27 K. T. Butler, D. W. Davies, H. Cartwright, O. Isayev and A. Walsh, *Nature*, 2018, **559**, 547–555.

28 J. A. Keith, V. Vassilev-Galindo, B. Cheng, S. Chmiela, M. Gastegger, K. R. Müller and A. Tkatchenko, *Chem. Rev.*, 2021, **121**, 9816–9872.

29 R. Ramprasad, R. Batra, G. Pilania, A. Mannodi-Kanakkithodi and C. Kim, *npj Comput. Mater.*, 2017, **3**, 1–13.

30 W. Sha, Y. Li, S. Tang, J. Tian, Y. Zhao, Y. Guo, W. Zhang, X. Zhang, S. Lu, Y. Cao and S. Cheng, *InfoMat*, 2021, **3**, 353–361.

31 T. Xie, A. France-Lanord, Y. Wang, Y. Shao-Horn and J. C. Grossman, *Nat. Commun.*, 2019, **10**, 1–9.

32 D. Nguyen, L. Tao and Y. Li, *Front. Chem.*, 2022, **9**, 1–26.

33 H. Yamada, C. Liu, S. Wu, Y. Koyama, S. Ju, J. Shiomi, J. Morikawa and R. Yoshida, *ACS Cent. Sci.*, 2019, **5**, 1717–1730.

34 K. Hatakeyama-Sato, T. Tezuka, M. Umeki and K. Oyaizu, *J. Am. Chem. Soc.*, 2020, **142**, 3301–3305.

35 G. Yang, M. L. Lehmann, S. Zhao, B. Li, S. Ge, P. F. Cao, F. M. Delnick, A. P. Sokolov, T. Saito and J. Nanda, *Energy Storage Mater.*, 2021, **35**, 431–442.

36 M. E. Günay, N. A. Tapan and G. Akkoç, *Int. J. Hydrogen Energy*, 2022, **47**, 2134–2151.

37 M. Olivecrona, T. Blaschke, O. Engkvist and H. Chen, *J. Cheminform.*, 2017, **9**, 1–14.

38 R. S. Sutton and A. G. Barto, *Reinforcement Learning: An Introduction*, MIT Press, Cambridge, MA, 2nd edn, 2018, p. 526.

39 P. Leinen, M. Esders, K. T. Schütt, C. Wagner, K. R. Müller and F. Stefan Tautz, *Sci. Adv.*, 2020, **6**(36), eabb6987.

40 T. Hatie, R. Tibshirani and J. Friedman, *The elements of statistical learning: data mining, inference, and prediction*, Springer, New York, 2009, p. 745.

41 Q. Wang, Y. Ma, K. Zhao and Y. Tian, *Ann. Data Sci.*, 2022, **9**, 187–212.

42 K. P. Murphy, *Machine learning: a probalistic perspective.* MIT Press, 2012, p. 1049.

43 A. Mardt, L. Pasquali, H. Wu and F. Noé, *Nat. Commun.*, 2018, **9**, 1–11.

44 S. Russell, *Artificial Intelligence a modern approach*, Pearson Education, Inc., 2010.

45 I. Goodfellow, Y. Bengio and A. Courville, *Deep Learning*, MIT Press, Cambridge, MA, 2016, pp. 164–223.

46 D. Duvenaud, D. Maclaurin, J. Aguilera-Iparraguirre, R. Gomez-Bombarelli, T. Hirzel, A. Aspuru-Guzik and R. P. Adams, *Adv. Neural Inf. Process. Syst.*, 2015, **2**, 2224–2232, DOI: 10.48550/arXiv.1509.09292.

47 B. Sanchez-Lengeling, E. Reif, A. Pearce and A. B. Wiltschko, *Distill*, 2021, **6**, e33.

48 T. Xie and J. C. Grossman, *J. Chem. Phys.*, 2018, **149**, 174111.

49 C. W. Coley, W. Jin, L. Rogers, T. F. Jamison, T. S. Jaakkola, W. H. Green, R. Barzilay and K. F. Jensen, *Chem. Sci.*, 2019, **10**, 370–377.

50 S. Batzner, A. Musaelian, L. Sun, M. Geiger, J. P. Mailoa, M. Kornbluth, N. Molinari, T. E. Smidt and B. Kozinsky, *Nat. Commun.*, 2022, **13**(1), 2453.

51 I. J. Goodfellow, J. Pouget-Abadie, M. Mirza, B. Xu, D. Warde-Farley, S. Ozair, A. Courville and Y. Bengio, *Commun. ACM*, 2020, **63**(11), 139–144.

52 P. Isola, J. Y. Zhu, T. Zhou and A. A. Efros, *Proc. - 30th IEEE Conf. Comput. Vis. Pattern Recognition*, 2017, pp. 1125–1134.

53 C. Donahue, J. McAuley, M. Puckette, *7th Int. Conf. Learn. Represent, arXiv*, 2018, preprint, arXiv:1802.04208, DOI: 10.48550/arXiv.1802.04208.

54 Y. Ganin, E. Ustinova, H. Ajakan, P. Germain, H. Larochelle, F. Laviolette, M. Marchand and V. Lempitsky, *J. Mach. Learn. Res.*, 2016, **17**, 1–35.

55 B. Kim, S. Lee and J. Kim, *Sci. Adv.*, 2020, **6**(1), eaax9324.

56 K. Hiraide, K. Hirayama, K. Endo and M. Muramatsu, *Comput. Mater. Sci.*, 2021, **190**, 110278.

57 Z. Yang, C. H. Yu and M. J. Buehler, *Sci. Adv.*, 2021, **7**(15), eabd7416.

58 G. J. Gilbert, D. C. Fabrycky, M. Stieffenhofer, M. Wand and T. Bereau, *Mach. Learn. Sci. Technol.*, 2020, **1**, 045014.

59 D. P. Kingma and M. Welling, *Found. Trends Mach. Learn.*, 2019, **12**, 307–392.

60 D. P. Kingma and M. Welling, 2013, preprint, arXiv:1312.6114, DOI: 10.48550/arXiv.1312.6114.

61 R. Pollice, G. Dos Passos Gomes, M. Aldeghi, R. J. Hickman, M. Krenn, C. Lavigne, M. Lindner-D'Addario, A. Nigam, C. T. Ser, Z. Yao and A. Aspuru-Guzik, *Acc. Chem. Res.*, 2021, **54**, 849–860.

62 J. C. Chen, J. P. Chen, M. W. Shen, M. Wornow, M. Bae, W. H. Yeh, A. Hsu and D. R. Liu, *Nat. Commun.*, 2022, **13**(1), 4541.

63 P. B. Jørgensen, M. Mesta, S. Shil, J. M. García Lastra, K. W. Jacobsen, K. S. Thygesen and M. N. Schmidt, *J. Chem. Phys.*, 2018, **148**, 241735.

64 Z. Yao, B. Sánchez-Lengeling, N. S. Bobbitt, B. J. Bucior, S. G. H. Kumar, S. P. Collins, T. Burns, T. K. Woo, O. K. Farha, R. Q. Snurr and A. Aspuru-Guzik, *Nat. Mach. Intell.*, 2021, **3**(1), 76–86.

65 W. Wang and R. Gómez-Bombarelli, *npj Comput. Mater.*, 2019, **5**(1), 125.

66 J. L. Elman, *Cogn. Sci.*, 1990, **14**, 179–211.

67 A. T. Müller, J. A. Hiss and G. Schneider, *J. Chem. Inf. Model.*, 2018, **58**, 472–479.

68 S. Karita, N. Chen, T. Hayashi, T. Hori, H. Inaguma, Z. Jiang, M. Someki, N. E. Y. Soplin, R. Yamamoto, X. Wang, S. Watanabe, T. Yoshimura and W. Zhang, *2019 IEEE Autom. Speech Recognit. Underst. Work. ASRU 2019 - Proc.*, 2019, pp. 449–456.

69 E. J. Bjerrum, *arXiv*, 2017, preprint, arXiv:1703.07076, DOI: 10.48550/arXiv.1703.07076.

70 A. L. Nazarova, L. Yang, K. Liu, A. Mishra, R. K. Kalia, K. I. Nomura, A. Nakano, P. Vashishta and P. Rajak, *J. Chem. Inf. Model.*, 2021, **61**, 2175–2186.

71 R. Ma and T. Luo, *J. Chem. Inf. Model.*, 2020, **60**, 4684–4690.

72 O. Vandans, K. Yang, Z. Wu and L. Dai, *Phys. Rev. E*, 2020, **101**, 022502.

73 J. Andrews, O. Gkountouna and E. Blaisten-Barojas, *Chem. Sci.*, 2022, **13**, 7021–7033.

74 L. Simine, T. C. Allen and P. J. Rossky, *Proc. Natl. Acad. Sci. U. S. A.*, 2020, **117**, 13945–13948.

75 A. Vaswani, N. Shazeer, N. Parmar, J. Uszkoreit, L. Jones, A. N. Gomez, Ł. Kaiser and I. Polosukhin, *Adv. Neural Inf. Process. Syst.*, 2017, 5999–6009.

76 J. Devlin, M. W. Chang, K. Lee and K. Toutanova, *NAACL HLT 2019 - 2019 Conf. North Am. Chapter Assoc. Comput. Linguist. Hum. Lang. Technol. - Proc. Conf.*, 2018, vol. 1, pp. 4171–4186.

77 Y. Liu, M. Ott, N. Goyal, J. Du, M. Joshi, D. Chen, O. Levy, M. Lewis, L. Zettlemoyer and V. Stoyanov, *arXiv*, 2019, preprint, arXiv:1907.11692, DOI: 10.48550/arXiv.1907.11692.

78 M. Lewis, Y. Liu, N. Goyal, M. Ghazvininejad, A. Mohamed, O. Levy, V. Stoyanov and L. Zettlemoyer, *arXiv*, 2019, preprint, arXiv:1910.13461, DOI: 10.48550/arXiv.1910.13461.

79 R. Irwin, S. Dimitriadis, J. He and E. J. Bjerrum, *Mach. Learn. Sci. Technol.*, 2022, **3**, 015022.

80 S. Chithrananda, G. Grand and B. Ramsundar, *arXiv*, 2020, preprint, arXiv:2010.09885, DOI: 10.48550/arXiv.2010.09885.

81 C. Xu, Y. Wang and A. Barati Farimani, *npj Comput. Mater.*, 2023, **9**(1), 64.

82 C. Kuenneth and R. Ramprasad, *Nat. Commun.*, 2023, **14**(1), 4099.

83 J. Görtler, R. Kehlbeck and O. Deussen, *Distill*, 2019, **4**, e17.

84 C. E. Rasmussen and C. K. I. Williams, *Gaussian Processes for Machine Learning*, MIT Press, Cambridge, MA, 2006, vol. 2, no. 3.

85 X. Du, L. Lüer, T. Heumueller, J. Wagner, C. Berger, T. Osterrieder, J. Wortmann, S. Langner, U. Vongsaysy, M. Bertrand, N. Li, T. Stubhan, J. Hauch and C. J. Brabec, *Joule*, 2021, **5**, 495–506.

86 L. Tao, V. Varshney and Y. Li, *J. Chem. Inf. Model.*, 2021, **61**, 5395–5413.

87 Y. Zhang and X. Xu, *Polym. Chem.*, 2021, **12**, 843–851.

88 L. Chen, C. Kim, R. Batra, J. P. Lightstone, C. Wu, Z. Li, A. A. Deshmukh, Y. Wang, H. D. Tran, P. Vashishta, G. A. Sotzing, Y. Cao and R. Ramprasad, *npj Comput. Mater.*, 2020, **6**(1), 61.

89 S. A. Lopez, B. Sanchez-Lengeling, J. de Goes Soares and A. Aspuru-Guzik, *Joule*, 2017, **1**, 857–870.

90 H. L. Morgan, *J. Chem. Doc.*, 1965, **5**, 107–113.

91 Z. Ma, S. Wang, M. Kim, K. Liu, C. L. Chen and W. Pan, *Soft Matter*, 2021, **17**, 5864–5877.

92 W. S. Noble, *Nat. Biotechnol.*, 2006, **24**(12), 1565–1567.

93 V. N. Vapnik, *The Nature of Statistical Learning Theory*, Springer Science and Business Media, 1999.

94 G. Konstantopoulos, E. P. Koumoulos and C. A. Charitidis, *Mater. Des.*, 2020, **192**, 108705.

95 C. Boztepe, A. Künkül and M. Yüceer, *J. Drug Delivery Sci. Technol.*, 2020, **57**, 101603.

96 C. Higuchi, D. Horvath, G. Marcou, K. Yoshizawa and A. Varnek, *ACS Appl. Polym. Mater.*, 2019, **1**, 1430–1442.

97 H. Ziaee, S. M. Hosseini, A. Sharafpoor, M. Fazavi, M. M. Ghiasi and A. Bahadori, *J. Taiwan Inst. Chem. Eng.*, 2015, **46**, 205–213.

98 P. I. Frazier, *arXiv*, 2018, preprint, arXiv:1807.02811, DOI: 10.48550/arXiv.1807.02811.

99 H. Zhai and J. Yeo, *ACS Biomater. Sci. Eng.*, 2023, **9**, 269–279.

100 A. Biswas, A. N. Morozovska, M. Ziatdinov, E. A. Eliseev and S. V. Kalinin, *J. Appl. Phys.*, 2021, **130**, 204102.

101 Y. Zhang, D. W. Apley and W. Chen, *Sci. Rep.*, 2020, **10**(1), 4924.

102 S. Diwale, M. K. Eisner, C. Carpenter, W. Sun, G. C. Rutledge and R. D. Braatz, *Mol. Syst. Des. Eng.*, 2022, **7**, 622–636.

103 Q. Zhu, V. Sharma, A. R. Oganov and R. Ramprasad, *J. Chem. Phys.*, 2014, **141**, 154102.

104 Q. Liang, A. E. Gongora, Z. Ren, A. Tiihonen, Z. Liu, S. Sun, J. R. Deneault, D. Bash, F. Mekki-Berrada, S. A. Khan, K. Hippalgaonkar, B. Maruyama, K. A. Brown, J. Fisher and T. Buonassisi, *npj Comput. Mater.*, 2021, **7**(1), 188.

105 C. Kim, A. Chandrasekaran, A. Jha and R. Ramprasad, *MRS Commun.*, 2019, **9**, 860–866.

106 R. Mercado, R. S. Fu, A. V. Yakutovich, L. Talirz, M. Haranczyk and B. Smit, *Chem. Mater.*, 2018, **30**, 5069–5086.

107 A. Deshwal, C. M. Simon and J. R. Doppa, *Mol. Syst. Des. Eng.*, 2021, **6**, 1066–1086.

108 D. Shin, A. Cupertino, M. H. J. de Jong, P. G. Steeneken, M. A. Bessa and R. A. Norte, *Adv. Mater.*, 2022, **34**, 2106248.

109 D. Khatamsaz, A. Molkeri, R. Couperthwaite, J. James, R. Arróyave, A. Srivastava and D. Allaire, *Mater. Des.*, 2021, **209**, 110001.

110 D. Khatamsaz, A. Molkeri, R. Couperthwaite, J. James, R. Arróyave, D. Allaire and A. Srivastava, *Acta Mater.*, 2021, **206**, 116619.

111 R. Nakayama, R. Shimizu, T. Haga, T. Kimura, Y. Ando, S. Kobayashi, N. Yasuo, M. Sekijima and T. Hitosugi, *Sci. Technol. Adv. Mater.: Methods*, 2022, **2**(1), 119–128.

112 H. Bellamy, A. A. Rehim, O. I. Orhobor and R. King, *J. Chem. Inf. Model.*, 2022, **62**, 3970–3981.

113 C. Li, D. Rubín De Celis Leal, S. Rana, S. Gupta, A. Sutti, S. Greenhill, T. Slezak, M. Height and S. Venkatesh, *Sci. Rep.*, 2017, **7**(1), 1–10.

114 H. Gao, S. Zhong, W. Zhang, T. Igou, E. Berger, E. Reid, Y. Zhao, D. Lambeth, L. Gan, M. A. Afolabi, Z. Tong, G. Lan and Y. Chen, *Environ. Sci. Technol.*, 2022, **56**, 2572–2581.

115 Y. Wang, T. Xie, A. France-Lanord, A. Berkley, J. A. Johnson, Y. Shao-Horn and J. C. Grossman, *Chem. Mater.*, 2020, **32**, 4144–4151.

116 D. Whitley, *Stat. Comput.*, 1994, **4**, 65–85.

117 H. M. Cartwright, R. M. Gunatillake and L. Sztandera, *Proc. - Int. Work. Database Expert Syst. Appl. DEXA*, 2006, pp. 598–602.

118 D. Weininger, *J. Chem. Inf. Comput. Sci.*, 1988, **28**, 31–36.

119 V. Meenakshisundaram, J. H. Hung, T. K. Patra and D. S. Simmons, *Macromolecules*, 2017, **50**, 1155–1166.

120 C. Kim, R. Batra, L. Chen, H. Tran and R. Ramprasad, *Comput. Mater. Sci.*, 2021, **186**, 110067.

121 J. Kern, L. Chen, C. Kim and R. Ramprasad, *J. Mater. Sci.*, 2021, **56**, 19623–19635.

122 R. W. Smith, *Comput. Phys. Commun.*, 1992, **71**, 134–146.

123 K. Kim, P. A. Graf and W. B. Jones, *J. Comput. Phys.*, 2005, **208**, 735–760.

124 S. V. Dudiy and A. Zunger, *Phys. Rev. Lett.*, 2006, **97**, 046401.

125 N. K. Roy, W. D. Potter and D. P. Landau, *Appl. Intell.*, 2004, **20**, 215–229.

126 S. Manos, M. C. J. Large and L. Poladian, *Proc. GECCO 2007 Genet. Evol. Comput. Conf. Companion Mater.*, 2007, pp. 2549–2556.

127 K. R. Fowler, E. W. Jenkins, C. L. Cox, B. McClune and B. Seyfzadeh, *Sep. Sci. Technol.*, 2008, **43**(4), 710–726.

128 A. Mannodi-Kanakkithodi, G. Pilania, T. D. Huan, T. Lookman and R. Ramprasad, *Sci. Rep.*, 2016, **6**, 1–10.

129 J. Kennedy and R. Eberhart, *Proc. ICNN'95 - Int. Conf. Neural Networks*, 1995, **4**, 1942–1948.

130 Y. Shi and R. Eberhart, *Proc. IEEE Conf. Evol. Comput. ICEC*, 1998, 69–73.

131 A. Tam, *A Gentle Introduction to Particle Swarm Optimization*, 2021, https://machinelearningmastery.com/a-gentle-introduction-to-particle-swarm-optimization/.

132 M. Shokooh-Saremi and R. Magnusson, *Opt. Lett.*, 2007, **32**(8), 894–896.

133 Y. Wang, M. Miao, J. Lv, L. Zhu, K. Yin, H. Liu and Y. Ma, *J. Chem. Phys.*, 2012, **137**, 224108.

134 Y. Wang, J. Lv, L. Zhu and Y. Ma, *Phys. Rev. B: Condens. Matter Mater. Phys.*, 2010, **82**, 094116.

135 X. Y. Kou, G. T. Parks and S. T. Tan, *Comput. Des.*, 2012, **44**, 300–310.

136 V. Savsani, R. V. Rao and D. P. Vakharia, *Mech. Mach. Theory*, 2010, **45**, 531–541.

137 G. C. Luh and C. Y. Lin, *Comput. Struct.*, 2011, **89**, 2221–2232.

138 M. R. Khadilkar, S. Paradiso, K. T. Delaney and G. H. Fredrickson, *Macromolecules*, 2017, **50**, 6702–6709.

139 J. N. Kumar, Q. Li, K. Y. T. Tang, T. Buonassisi, A. L. Gonzalez-Oyarce and J. Ye, *npj Comput. Mater.*, 2019, **5**(1), 73.

140 M. B. Francisco, D. M. Junqueira, G. A. Oliver, J. L. J. Pereira, S. S. da Cunha and G. F. Gomes, *Eng. Optim.*, 2020, **53**(11), 1922–1945.

141 B. O. P. Soepangkat, R. Norcahyo, M. K. Effendi and B. Pramujati, *Int. J. Eng. Sci. Technol.*, 2020, **23**, 700–713.

142 L. J. Case, K. T. Delaney, G. H. Fredrickson, F. S. Bates and K. D. Dorfman, *Eur. Phys. J. E*, 2021, **44**, 115.

143 C. L. Tsai and G. H. Fredrickson, *Macromolecules*, 2022, **22**, 44.

144 S. Ibrahim and M. R. Johan, *Int. J. Electrochem. Sci.*, 2011, **6**, 5565–5587.

145 G. Bradford, J. Lopez, J. Ruza, M. A. Stolberg, R. Osterude, J. A. Johnson, R. Gomez-Bombarelli and Y. Shao-Horn, *ACS Cent. Sci.*, 2023, **9**(2), 206–216.

146 W. Kohn and L. J. Sham, *Phys. Rev.*, 1965, **140**, A1133.

147 S. H. Vosko and L. Wilk, *Phys. Rev. B: Condens. Matter Mater. Phys.*, 1980, **22**, 3812.

148 K. Burke, J. P. Perdew and Y. Wang, *Electronic Density Functional Theory: Recent Progress and New Directions*, Springer US, Boston, MA, 1998, pp. 81–111.

149 Y. Zhao and D. G. Truhlar, *Theor. Chem. Acc.*, 2008, **120**, 215–241.

150 J. Da Chai and M. Head-Gordon, *J. Chem. Phys.*, 2008, **128**(8), 084106.

151 A. D. Becke, *Phys. Rev. A: At., Mol., Opt. Phys.*, 1988, **38**, 3098.

152 C. Lee, W. Yang and R. G. Parr, *Phys. Rev. B: Condens. Matter Mater. Phys.*, 1988, **37**, 785.

153 D. S. Sholl and J. A. Steckel, *Density functional theory: a practical introduction*, John Wiley & Sons, 2022.

154 F. Giustino, *Materials modelling using density functional theory: properties and predictions*, Oxford University Press, 2014.

155 M. Bursch, J. M. Mewes, A. Hansen and S. Grimme, *Angew. Chem., Int. Ed.*, 2022, **61**, e202205735.

156 L. Chen, S. Venkatram, C. Kim, R. Batra, A. Chandrasekaran and R. Ramprasad, *Chem. Mater.*, 2019, **31**, 4598–4604.

157 C. F. N. Marchiori, R. P. Carvalho, M. Ebadi, D. Brandell and C. M. Araujo, *Chem. Mater.*, 2020, **32**, 7237–7246.

158 M. Unge, H. Gudla, C. Zhang and D. Brandell, *Phys. Chem. Chem. Phys.*, 2020, **22**, 7680–7684.

159 M. Ebadi, C. Marchiori, J. Mindemark, D. Brandell and C. M. Araujo, *J. Mater. Chem. A*, 2019, **7**, 8394–8404.

160 A. Mannodi-Kanakkithodi and M. K. Y. Chan, *Trends Chem.*, 2021, **3**, 79–82.

161 G. R. Schleder, A. C. M. Padilha, C. M. Acosta, M. Costa and A. Fazzio, *J. Phys. Mater.*, 2019, **2**, 032001.

162 G. Åvall, J. Mindemark, D. Brandell, P. Johansson, G. Åvall, P. Johansson, J. Mindemark and D. Brandell, *Adv. Energy Mater.*, 2018, **8**, 1703036.

163 C. Ling, *npj Comput. Mater.*, 2022, **8**, 33.

164 K. Li, J. Wang, Y. Song and Y. Wang, *Nat. Commun.*, 2023, **14**(1), 2789.

165 A. Jain, S. P. Ong, G. Hautier, W. Chen, W. D. Richards, S. Dacek, S. Cholia, D. Gunter, D. Skinner, G. Ceder and K. A. Persson, *APL Mater.*, 2013, **1**, 011002.

166 S. Curtarolo, W. Setyawan, S. Wang, J. Xue, K. Yang, R. H. Taylor, L. J. Nelson, G. L. W. Hart, S. Sanvito, M. Buongiorno-Nardelli, N. Mingo and O. Levy, *Comput. Mater. Sci.*, 2012, **58**, 227–235.

167 S. Kirklin, J. E. Saal, B. Meredig, A. Thompson, J. W. Doak, M. Aykol, S. Rühl and C. Wolverton, *npj Comput. Mater.*, 2015, **1**, 1–15.

168 S. S. Borysov, R. M. Geilhufe and A. V. Balatsky, *PLoS One*, 2017, **12**, e0171501.

169 L. Lin, *Mater. Perform. Charact.*, 2015, **4**, 148–169.

170 D. Diddens, W. A. Appiah, Y. Mabrouk, A. Heuer, T. Vegge, A. Bhowmik, D. Diddens, Y. Mabrouk, A. Heuer, W. A. Appiah, T. Vegge and A. Bhowmik, *Adv. Mater. Interfaces*, 2022, **9**, 2101734.

171 R. Iftimie, P. Minary and M. E. Tuckerman, *Proc. Natl. Acad. Sci. U. S. A.*, 2005, **102**, 6654–6659.

172 A. Musaelian, S. Batzner, A. Johansson, L. Sun, C. J. Owen, M. Kornbluth and B. Kozinsky, *Nat. Commun.*, 2023, **14**(1), 579.

173 X. Fu, Z. Wu, W. Wang, T. Xie, M. Research, R. Gomez-Bombarelli and T. Jaakkola, 2022, preprint, arXiv:2210.07237, DOI: **10.48550/arXiv.2210.07237**.

174 P. Friederich, F. Häse, J. Proppe and A. Aspuru-Guzik, *Nat. Mater.*, 2021, **20**, 750–761.

175 P. O. Dral, *J. Phys. Chem. Lett.*, 2020, **11**, 2336–2347.

176 C. Zhai, T. Li, H. Shi and J. Yeo, *J. Mater. Chem. B*, 2020, **8**, 6562–6587.

177 J. Behler and M. Parrinello, *Phys. Rev. Lett.*, 2007, **98**, 146401.

178 J. Behler, *Int. J. Quantum Chem.*, 2015, **115**, 1032–1050.

179 J. Behler, *J. Chem. Phys.*, 2011, **134**, 074106.

180 J. S. Smith, O. Isayev and A. E. Roitberg, *Chem. Sci.*, 2017, **8**, 3192–3203.

181 C. Devereux, J. S. Smith, K. K. Davis, K. Barros, R. Zubatyuk, O. Isayev and A. E. Roitberg, *J. Chem. Theory Comput.*, 2020, **16**, 4192–4202.

182 S. A. Ghasemi, A. Hofstetter, S. Saha and S. Goedecker, *Phys. Rev. B: Condens. Matter Mater. Phys.*, 2015, **92**, 045131.

183 S. Faraji, S. A. Ghasemi, S. Rostami, R. Rasoulkhani, B. Schaefer, S. Goedecker and M. Amsler, *Phys. Rev. B*, 2017, **95**, 104105.

184 E. R. Khajehpasha, J. A. Finkler, T. D. Kühne and S. A. Ghasemi, *Phys. Rev. B*, 2022, **105**, 144106.

185 M. Gastegger, L. Schwiedrzik, M. Bittermann, F. Berzsenyi and P. Marquetand, *J. Chem. Phys.*, 2018, **148**, 241709.

186 A. P. Bartók, M. C. Payne, R. Kondor and G. Csányi, *Phys. Rev. Lett.*, 2010, **104**, 136403.

187 A. P. Bartók, R. Kondor and G. Csányi, *Phys. Rev. B: Condens. Matter Mater. Phys.*, 2013, **87**, 184115.

188 M. Rupp, A. Tkatchenko, K. R. Müller and O. A. Von Lilienfeld, *Phys. Rev. Lett.*, 2012, **108**, 058301.

189 J. Behler, *Chem. Rev.*, 2021, **121**, 10037–10072.

190 J. Behler, *J. Chem. Phys.*, 2016, **145**, 170901.

191 K. Yao, J. E. Herr, D. W. Toth, R. McKintyre and J. Parkhill, *Chem. Sci.*, 2018, **9**, 2261–2269.

192 M. Wen and E. B. Tadmor, *npj Comput. Mater.*, 2020, **6**(1), 124.

193 A. V. Shapeev, *Multiscale Model. Simul.*, 2016, **14**, 1153–1173.

194 L. Zhang, J. Han, H. Wang, R. Car and E. Weinan, *Phys. Rev. Lett.*, 2018, **120**, 143001.

195 O. T. Unke and M. Meuwly, *J. Chem. Theory Comput.*, 2019, **15**, 3678–3693.

196 G. N. Simm, J. Proppe and M. Reiher, *arXiv*, 2017, preprint, arXiv:1702.00867, DOI: **10.48550/arXiv.1702.00867**.

197 R. J. Brachman, W. W. Cohen, T. G. Dietterich and B. Settles, *Synth. Lect. Artif. Intell. Mach. Learn.*, 2012, **18**, 1–111.

198 A. Paszke, S. Gross, F. Massa, A. Lerer, J. Bradbury, G. Chanan, T. Killeen, Z. Lin, N. Gimelshein, L. Antiga, A. Desmaison, A. Köpf, E. Yang, Z. DeVito, M. Raison, A. Tejani, S. Chilamkurthy, B. Steiner, L. Fang, J. Bai and S. Chintala, *Adv. Neural Inf. Process. Syst.*, 2019, **32**, 8026–8037.

199 X. Gao, F. Ramezanghorbani, O. Isayev, J. S. Smith and A. E. Roitberg, *J. Chem. Inf. Model.*, 2020, **60**, 3408–3415.

200 J. S. Smith, R. Zubatyuk, B. Nebgen, N. Lubbers, K. Barros, A. E. Roitberg, O. Isayev and S. Tretiak, *Sci. Data*, 2020, **7**, 134.

201 H. Wang, L. Zhang, J. Han and W. E, *Comput. Phys. Commun.*, 2018, **228**, 178–184.

202 R. Zubatyuk, J. S. Smith, J. Leszczynski and O. Isayev, *Sci. Adv.*, 2019, **5**(8), eaav6490.

203 G. Csanyi, S. Winfield, J. Kermode, M. C. Payne, A. Comisso, A. De Vita and N. Bernstein, *Newsl. Comput. Phys. Group*, 2007, 1–24.

204 A. P. Bartók and G. Csányi, *Int. J. Quantum Chem.*, 2015, **115**, 1051–1057.

205 J. Behler, *Angew. Chem., Int. Ed.*, 2017, **56**, 12828–12840.

206 T. W. Ko, J. A. Finkler, S. Goedecker and J. Behler, *Nat. Commun.*, 2021, **12**(1), 398.

207 E. B. Tadmor, R. S. Elliott, J. P. Sethna, R. E. Miller and C. A. Becker, *JOM*, 2011, **63**, 17.

208 F. Noé, A. Tkatchenko, K. R. Müller and C. Clementi, *Annu. Rev. Phys. Chem.*, 2020, **71**, 361–390.

209 A. Rahman, P. Deshpande, M. S. Radue, G. M. Odegard, S. Gowtham, S. Ghosh and A. D. Spear, *Compos. Sci. Technol.*, 2021, **207**, 108627.

210 X. Meng, Y. Liu, Y. Ma, Y. Boyjoo, J. Liu, J. Qiu, Z. Wang, X. Meng, Y. Liu, Z. Wang, Y. Ma, Y. Boyjoo, J. Liu and J. Qiu, *Adv. Mater.*, 2023, **35**, 2212039.

211 M. Yao, Q. Ruan, S. Pan, H. Zhang and S. Zhang, *Adv. Energy Mater.*, 2023, **13**, 2203640.

212 R. Rojaee, S. Cavallo, S. Mogurampelly, B. K. Wheatle, V. Yurkiv, R. Deivanayagam, T. Foroozan, M. Golam Rasul, S. Sharifi-Asl, A. H. Phakatkar, M. Cheng, S.-B. Son, Y. Pan, F. Mashayek, V. Ganesan, R. Shahbazian-Yassar, R. Rojaee, S. Cavallo, V. Yurkiv, R. Deivanayagam, T. Foroozan, M. G. Rasul, S. Sharifi-Asl, M. Cheng, Y. Pan, F. Mashayek, R. Shahbazian-Yassar, S. Mogurampelly,

B. K. Wheatle, V. Ganesan, A. H. Phakatkar and S. Son, *Adv. Funct. Mater.*, 2020, **30**, 1910749.

213 D. J. Wales and T. V. Bogdan, *J. Phys. Chem. B*, 2006, **110**, 20765–20776.

214 M. Gruebele, *Curr. Opin. Struct. Biol.*, 2002, **12**, 161–168.

215 L. Mones, N. Bernstein and G. Csányi, *J. Chem. Theory Comput.*, 2016, **12**, 5100–5110.

216 G. H. Teichert, A. R. Natarajan, A. Van der Ven and K. Garikipati, *Comput. Methods Appl. Mech. Eng.*, 2019, **353**, 201–216.

217 A. Volkhardt and H. Grubmüller, *Phys. Rev. E*, 2022, **105**, 044404.

218 E. Schneider, L. Dai, R. Q. Topper, C. Drechsel-Grau and M. E. Tuckerman, *Phys. Rev. Lett.*, 2017, **119**, 150601.

219 H. Fu, H. Chen, M. Blazhynska, E. Goulard Coderc de Lacam, F. Szczepaniak, A. Pavlova, X. Shao, J. C. Gumbart, F. Dehez, B. Roux, W. Cai and C. Chipot, *Nat. Protoc.*, 2022, **17**(4), 1114–1141.

220 G. Bussi and A. Laio, *Nat. Rev. Phys.*, 2020, **2**(4), 200–212.

221 T. Stecher, N. Bernstein and G. Csányi, *J. Chem. Theory Comput.*, 2014, **10**, 4079–4097.

222 R. Fabregat, A. Fabrizio, E. A. Engel, B. Meyer, V. Juraskova, M. Ceriotti and C. Corminboeuf, *J. Chem. Theory Comput.*, 2022, **18**, 1467–1479.

223 H. Wu and F. Noé, *J. Nonlinear Sci.*, 2020, **30**, 23–66.

224 T. Xie and J. C. Grossman, *Phys. Rev. Lett.*, 2018, **120**, 145301.

225 C. W. Park and C. Wolverton, *Phys. Rev. Mater.*, 2020, **4**, 063801.

226 H. C. Yi, Z. H. You, D. S. Huang and C. K. Kwoh, *Briefings Bioinf.*, 2022, **23**, 1–16.

227 Y. Wang, J. Wang, Z. Cao and A. Barati Farimani, *Nat. Mach. Intell.*, 2022, **4**(3), 279–287.

228 S. Zhang, H. Tong, J. Xu and R. Maciejewski, *Comput. Soc. Networks*, 2019, **6**, 1–23.

229 F. Scarselli, M. Gori, A. C. Tsoi, M. Hagenbuchner and G. Monfardini, *IEEE Trans. Neural Networks*, 2009, **20**, 61–80.

230 T. Tsafack, J. M. Alred, K. E. Wise, B. Jensen, E. Siochi and B. I. Yakobson, *Carbon*, 2016, **105**, 600–606.

231 A. Eitan, K. Jiang, D. Dukes, R. Andrews and L. S. Schadler, *Chem. Mater.*, 2003, **15**, 3198–3201.

232 T. Xie, A. France-Lanord, Y. Wang, J. Lopez, M. A. Stolberg, M. Hill, G. M. Leverick, R. Gomez-Bombarelli, J. A. Johnson, Y. Shao-Horn and J. C. Grossman, *Nat. Commun.*, 2022, **13**(1), 3415.

233 J. Liu, D. Cao and L. Zhang, *J. Phys. Chem. C*, 2008, **112**, 6653–6661.

234 B. M. Aguilera-Mercado, C. Cohen and F. A. Escobedo, *Macromolecules*, 2014, **47**, 840–850.

235 M. Ghelichi, K. Malek and M. H. Eikerling, *Macromolecules*, 2016, **49**, 1479–1489.

236 M. S. Alshammasi and F. A. Escobedo, *Macromolecules*, 2018, **51**, 9213–9221.

237 C. L. Ting, M. J. Stevens and A. L. Frischknecht, *Macromolecules*, 2015, **48**, 809–818.

238 M. C. Tekell and S. K. Kumar, *Macromolecules*, 2021, **54**, 7160–7173.

239 R. D. Groot and P. B. Warren, *J. Chem. Phys.*, 1998, **107**, 4423.

240 A. Maiti and S. McGrother, *J. Chem. Phys.*, 2004, **120**, 1594.

241 C. F. Fan, B. D. Olafson, M. Blanco and S. L. Hsu, *Macromolecules*, 1992, **25**, 3667–3676.

242 R. D. Groot, *J. Chem. Phys.*, 2003, **118**, 11265.

243 M. T. Lee, *J. Phys. Chem. C*, 2019, **123**, 10802–10815.

244 W. G. Noid, *J. Phys. Chem. B*, 2023, **127**, 4174–4207.

245 S. Dhamankar and M. A. Webb, *J. Polym. Sci.*, 2021, **59**, 2613–2643.

246 C. I. Wang and N. E. Jackson, *Chem. Mater.*, 2023, **35**, 1470–1486.

247 J. Jin, A. J. Pak, A. E. P. Durumeric, T. D. Loose and G. A. Voth, *J. Chem. Theory Comput.*, 2022, **18**, 5759–5791.

248 X. Fu, T. Xie, N. J. Rebello, B. D. Olsen and T. Jaakkola, 2022, preprint, arXiv:2204.10348, DOI: **10.48550/arXiv.2204.10348**.

249 S. Liu, Y. Su, H. Yin, D. Zhang, J. He, H. Huang, X. Jiang, X. Wang, H. Gong, Z. Li, H. Xiu, J. Wan and X. Zhang, *npj Comput. Mater.*, 2021, **7**(1), 88.

250 B. G. Pelkie and L. D. Pozzo, *Digital Discovery*, 2023, **2**, 544–556.

251 S. Oliver, L. Zhao, A. J. Gormley, R. Chapman and C. Boyer, *Macromolecules*, 2019, **52**, 3–23.

252 R. MacArron, M. N. Banks, D. Bojanic, D. J. Burns, D. A. Cirovic, T. Garyantes, D. V. S. Green, R. P. Hertzberg, W. P. Janzen, J. W. Paslay, U. Schopfer and G. S. Sittampalam, *Nat. Rev. Drug Discovery*, 2011, **10**, 188–195.